Synthetic Models for Non-Heme Carboxylate-Bridged Diiron Metalloproteins: Strategies and Tactics

Edit Y. Tshuva and Stephen J. Lippard*

Department of Chemistry, Massachusetts Institute of Technology, Cambridge, Massachusetts 02139

Received August 13, 2003

Contents

* To whom correspondence should be addressed. E-mail: lippard@lippard.mit.edu.

1. Introduction—Nature's Inspiration

Metalloproteins perform a variety of functions in biological systems. The catalysis of several remarkable chemical transformations occurs at metal centers embedded in the active sites of metalloenzymes. Metalloproteins having carboxylate-bridged diiron cores comprise an important class, with functional versatility despite obvious structural similarities.[1−7] The functions performed by these proteins and their significance have inspired a range of biomimetic studies, which in turn suggest possible chemical, biological, and pharmaceutical applications.[1,8−11] The development of small molecule synthetic model compounds for non-heme dinuclear iron-based metalloproteins is a challenging field. In this article we review two decades of progress in the area.

Table 1 lists metalloproteins that have now been identified to share the carboxylate-bridged diiron active site motif.[3,4,6,7] Their various roles in nature are delineated. Some have been thoroughly investigated, and their X-ray structures are available. Examples include hemerythrin,[12] methane monooxygenase,[13,14] and ribonucleotide reductase.[15,16] Others are assigned to the carboxylate-bridged diiron family according to gene sequence analysis and, occasionally, available spectroscopic data.

The first carboxylate-bridged diiron protein to be discovered was hemerythrin (Hr), which has been studied since the 1950s.[12] Hemerythrins are dioxygen carrier proteins found in marine invertebrates. They are functional analogues of the mammalian proteins myoglobin and hemoglobin. The active site of hemerythrin (Scheme 1) is composed of two iron atoms bridged by two carboxylate ligands from glutamate and aspartate residues. Five terminally bound histidine units and a bridging hydroxo group complete the coordination spheres of the two iron atoms, one of which is six-coordinate and the other five-coordinate in the reduced, diiron(II) state of deoxy Hr. Upon reaction with O_2, deoxy Hr is converted to oxy Hr, in which an η^1-hydroperoxo group binds to the available coordination site and forms a hydrogen bond to the bridging oxo unit. Biomimetic studies of this protein have advanced the understanding of the mechanism

10.1021/cr020622y CCC: $48.50
Published on Web 01/21/2004

Edit Y. Tshuva (right) (born 1975) received her B. Sc. degree from Tel Aviv University in 1998, during which she worked with Professor Moshe Kol on boron–nitrogen compounds. She then continued toward graduate studies working in Professor Kol's laboratory in the field of organometallic chemistry, designing and investigating novel 1-olefin polymerization catalysts. She received her Ph. D. with distinction in 2001, and then joined Professor Lippard's laboratory holding the Fulbright fellowship. During her postdoctorate work, she conducted bioinorganic studies, working on the development and mechanistic understanding of functional models of soluble methane monooxygenase. Edit recently joined the department of inorganic and analytical chemistry in the Hebrew University of Jerusalem, Israel, as a senior lecturer.

Stephen J. Lippard (left) is Arthur Amos Noyes Professor of Chemistry and Head of the Chemistry Department at the Massachusetts Institute of Technology. His research activities span the fields of inorganic chemistry, biological chemistry, and neurochemistry. The synthesis and study of biomimetic compounds, the topic of this review, has for many years been a primary focus of attention in his laboratory. When he is not doing science you may encounter him jogging along the Charles River, playing the harpsichord, or at the movies.

Scheme 1

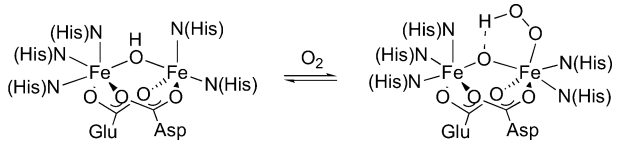

of dioxygen activation and transport in non-heme diiron centers in living aerobic systems.

Ribonucleotide reductases (RNRs),[15,17] one of which also contains a diiron active site in its R2 subunit (Scheme 2), catalyze the conversion of nucleotides to deoxynucleotides in the rate-determining step of the biosynthesis of DNA. Four types of RNRs have been

Scheme 2

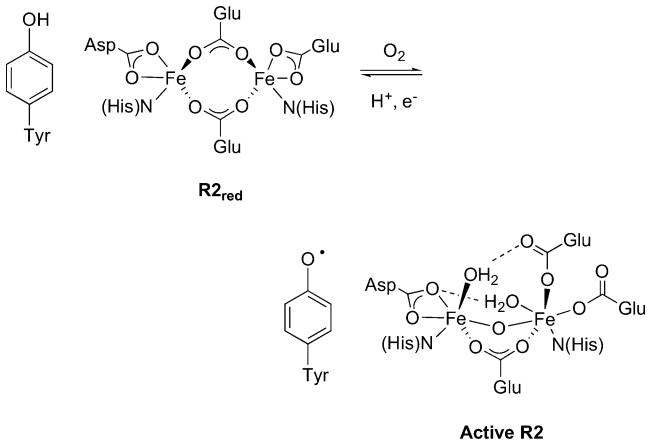

identified. The R2 active site of class I RNR, structurally characterized by X-ray crystallography,[16] has a dinuclear iron center which, in the reduced state, contains two bridging glutamate, one bidentate mononucleating glutamate, one bidentate mononucleating aspartate, and two terminal histidine ligands. Located in close proximity to this unit is the phenol side chain of a tyrosine residue. Upon reaction with dioxygen, the enzyme is functionally activated through the formation of a tyrosyl radical, and an oxo ligand bridges the two iron(III) atoms. The tyrosyl radical participates in electron transfer with the R1 subunit of RNR, initiating the eventual reduction of the ribose ring. The role of RNR enzymes in DNA biosynthesis makes them attractive targets for pharmaceutical applications such as antiviral and anticancer agents. Modeling their structure and reactivity through biomimetic chemistry may therefore contribute to the design of inhibitors based on carboxylate-bridged diiron chemistry.

Methane monooxygenases (MMOs)[13,18,19] are widely investigated metalloenzymes that catalyze the oxidation of methane to methanol by dioxygen. This unique function achieves the first step in the metabolism of methanotrophic bacteria, which consume methane and dioxygen as their sole source of carbon and energy. The active site of the hydroxylase component (MMOH) of soluble MMO (sMMO) (Figure 1) features a diiron center containing four glutamate and two histidine residues. The reduced state (H_{red}) is a diiron(II) form, whereas the oxidized, resting state (H_{ox}) houses a diiron(III) unit that usually contains

Table 1. Diiron Metalloproteins[3,4]

enzyme	function	method of characterization	ref
hemerythrin	dioxygen carrier	X-ray	12
ribonucleotide reductase	tyrosyl radical generator	X-ray	15, 16
methane monooxygenase	methane to methanol oxidation	X-ray	13, 14
purple acid phosphatase	phosphate ester hydrolysis	X-ray	158
ferritins	iron storage	X-ray	159
rubrerythrin	putative peroxidase	X-ray	160
Δ^9 desaturases	alkane conversion to alkene	X-ray	161
toluene monooxygenases	toluene to cresol oxidation	spectroscopy	4, 162
phenol hydroxylase	phenol to catechol oxidation	spectroscopy	163
alkene monooxygenase	alkene epoxidation	spectroscopy	164
butane monooxygenase	butane oxidation to butanol	sequence analysis	165
ω-alkane hydroxylase	alkane oxidation to alcohol	sequence analysis	166
DMQ monooxygenase	quinone generation	sequence analysis	167

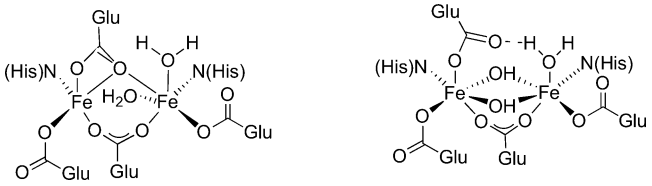

Figure 1. The active site of sMMO in its reduced (left) and oxidized (right) states.

Scheme 3

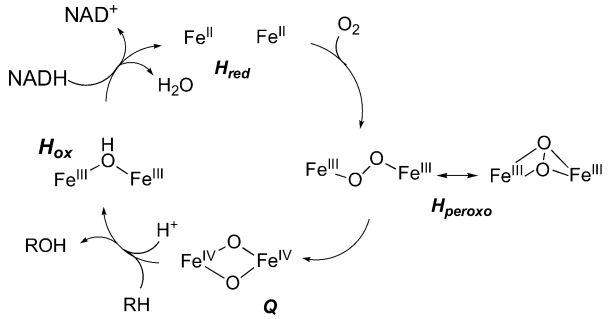

two bridging hydroxo ligands. Scheme 3 depicts minimal core transformations that occur during the MMOH catalytic cycle. The first spectroscopically characterized intermediate in the reaction of H_{ox} with O_2 is a peroxo species (H_{peroxo}), which subsequently converts to a high-valent di(μ-oxo)diiron(IV) component (Q). Intermediate Q reacts with methane, releasing the product methanol and generating a water molecule. The resulting resting diiron(III) state H_{ox} is reduced back to H_{red} by NADH via a reductase protein component MMOR, closing the cycle. A third protein MMOB couples electron transfer with efficient methane oxidation.[13]

The "monooxygenase" nomenclature is assigned to proteins that function to oxidize substrates in such a manner that one oxygen atom of the O_2 molecule is transferred to the substrate, while the other is reduced to form water. Thus, one molecule of substrate overall consumes one molecule of dioxygen. By contrast, oxidases are enzymes that catalyze the 4-electron reduction of dioxygen to water, and dioxygenases functionalize dioxygen such that the two oxygen atoms are transferred to a substrate. Thermodynamically, the enthalpic difference between reactions catalyzed by mono- and dioxygenases is, for methanol oxidation, formation of water, as indicated in eq 1. Since the free energy of formation of water at 298 K is negative ($\Delta G_f°$ [H_2O(l)] = −237.1 kJ/mol[20]), alkane oxidation by monooxygenases is facilitated by coupling the conversion of C−H to C−OH bonds with water formation.

Monooxygenase	$CH_4 + O_2 + H_2$	→	$CH_3OH + H_2O$	(1)
Dioxygenase	$CH_4 + 1/2\ O_2$	→	CH_3OH	
Difference	$H_2 + 1/2\ O_2$	→	H_2O	

In addition to methane, many other substrates react with sMMO. Included are long chain alkanes, alkenes, halogenated and other substituted alkanes, alkynes, sulfides, and others.[21−25] These reactions afford the synthetic model chemist a variety of possible substrates for which to mimic function. Chemical applications of functional MMO models are of potentially great importance; for example, the catalytic transformation of methane to methanol with O_2 under ambient conditions would bring about an economic revolution in the fuel industry.

Several other diiron metalloproteins are presented in Table 1. Like the few specific examples discussed above, their functions have also prompted synthetic model studies. Non-heme iron, including carboxylate-bridged diiron, chemistry in nature has, like heme systems, inspired many biomimetic studies. Included are ligand design, complex synthesis, structure elucidation, magnetic and spectroscopic characterization, and, of greatest interest, reactivity investigations, all integral components of bioinorganic chemistry. The body of this review is devoted to an analysis of this undertaking.

2. Introduction to Model Chemistry

Modeling the chemistry of non-heme diiron proteins is quite challenging.[8,9,11,26,27] In a typical protein, the active site is buried in a cavity surrounded by a heterophobic shield,[28] and the synthesis of small molecules capable of performing the same chemical transformation is formidable. The purpose of synthetic model chemistry is 2-fold. One goal is to mimic the function of an enzyme that catalyzes an important chemical transformation. The other is to gain scientific insight into the biological system, by providing mechanistic, structural, and spectroscopic data for comparison with those available for the macromolecule. This information may lead to better mimics, or even better drugs, depending upon the enzyme in question.[29] Moreover, a spectroscopic feature of a model compound that resembles one found for the enzyme in an intermediate state may assist in assigning its structure, advancing our understanding of the biological mechanism.[7,11]

As model chemists, our objectives often begin with organic synthesis and continue through several steps toward the ultimate goal of catalytic reactivity. At each stage there are difficulties, as described below.

2.1. Ligand Synthesis and Complex Formation

The initial goal in modeling the active site of a metalloenzyme is to synthesize an inorganic compound having structural and spectroscopic features as similar as possible to the active site in one of its stable states.[30] For many carboxylate-bridged diiron metalloenzymes, the reduced diiron(II) state is a most desirable target. Such compounds rarely assemble spontaneously upon mixing an iron(II) salt with carboxylate and other ligands to complete the coordination spheres.[31] Designing and synthesizing suitable dinucleating organic ligand precursors can therefore be a crucial first step, in which the following considerations must be addressed: (i) First and foremost, the ligands should have bridging potential, preferably through a carboxylate unit. The redox properties of the ligands should be compatible with diiron species in oxidation states II, III, and IV. Possible counterions need to be carefully chosen when a charged complex results. (ii) The steric properties

of the ligands are of great importance. Since the active site of the natural protein is protected by the polypeptide framework, one of the challenging tasks absent such an environment is to achieve dinuclearity, rather than mono- or polynuclear species.[31] Without sterically demanding groups, high nuclearity clusters are often obtained, whereas too much steric bulk will lead to mononuclear complexes. Steric factors must therefore be carefully chosen to tune the desired nuclearity. (iii) The coordination number of each iron atom in the resulting compound is also of importance. Since it is desirable that a diiron(II) complex react with dioxygen by coordination to the metal center, the envisioned diiron(II) compound should either be coordinatively unsaturated, or contain readily exchangeable ligands, such as water or other solvent components.

2.2. Reactivity with Dioxygen and Formation of Intermediates

Once a target dinuclear iron(II) complex is in hand and demonstrated to be a reasonable structural and spectroscopic mimic of a diiron metalloprotein active site, the next objective is to explore its chemical reactivity with an oxidant, preferably dioxygen. The generation of intermediates similar to those encountered with the natural systems will not only help to calibrate their assignment but may also ultimately lead to functional reactivity.[29,32] Several considerations are important in this respect. Since reactivity with dioxygen in biological systems often requires structural flexibility, such as carboxylate shifts,[1,33,34] this feature should be taken into account when designing model compounds and in studies of the mechanism of their dioxygen reactivity. Steric bulk may again play an important role, by facilitating or blocking such processes. Intraligand hydrogen bonding can promote the desired chemical transformation. Outside of the protein framework, it is possible that interesting intermediates are kinetically unstable, existing only at low temperatures. This problem may again be addressed by increasing steric bulk and/or H-bonding capacity to protect the metal center from decomposition. Alternatively, experiments can be performed at cryogenic temperatures. It is noteworthy that most aspects described above are not easy to control. The problems encountered are rarely anticipated, and the measures required to solve them can be difficult to execute. Many successful studies are the result of persistence.

2.3. The Oxidized Diiron(III) Resting State

Intermediates obtained upon reaction of carboxylate-bridged diiron(II) complexes with dioxygen typically convert ultimately to the diiron(III) state. Under favorable circumstances, the dinuclear structure is preserved, having a geometry analogous to that of the oxidized resting state of the protein. For RNR or Hr models, this species is a carboxylate-bridged (μ-oxo)diiron(III) complex, and for an MMOH model, a di(μ-hydroxo)diiron(III) species is desirable.[8] A different approach to these diiron(III) target compounds is their direct synthesis from iron(III) precursors. Formation of diiron(III) compounds from mononuclear starting materials upon exposure to a certain reagent, for example, reaction of an iron(II) complex with dioxygen or hydrogen peroxide, is also possible.

2.4. Functional Systems

A key objective is to model the reactivity of enzymes that catalyze substrate oxidation, such as methane monooxygenase, toluene monooxygenase, and related desaturases. Obtaining such a functional system requires the generation of a reactive intermediate with the redox potential and kinetic pathway required to oxidize the substrate selectively. It is hard to predict a priori which systems will have such properties and challenging to elucidate the mechanism of such a reaction when discovered. Knowledge of the mechanism is important for comparison to the ones taking place in the biological system. If the desired reactivity with a chosen substrate is obtained, elucidating the mechanism of that reaction is perhaps of lesser significance, especially if the reaction proceeds catalytically. But often one is not fortunate enough to oxidize the molecule of interest. For synthetic MMOH analogues, for example, oxidation of methane to methanol has yet to be achieved, and instead, one has to rely on information obtained from oxidizing alternative substrates. To the extent that such chemistry is similar to that encountered with the enzyme, however, valuable information can be obtained that enables the design of new and improved models.

Among several approaches to achieve functional mimics are the following: (i) to react a diiron(II) compound with dioxygen in the presence of the possible substrate; (ii) to react a diiron(III) compound with hydrogen peroxide for oxidation of the target substrate;[35] and (iii) to react a diiron(III) compound with an alkyl hydroperoxide (ROOH) or similar strong oxidant in the presence of substrate.[35] These approaches are listed in order of decreasing desirability as true functional mimics of the enzymes, all of which employ dioxygen under native conditions. The substrate can either be provided externally or tethered as a dangling fragment of a polyfunctional ligand. In the former case, it is advantageous to construct a substrate-binding cavity in the second coordination sphere.

2.5. Achieving Catalysis

The next and final objective is to mimic the catalytic activity obtained with the enzyme. For MMOH models, catalytically oxidizing methane to methanol would of course be the ultimate goal. Equation 2 illustrates the overall reaction, which is more general than eq 1 and does not require activation of H_2.

$$CH_4 + O_2 + 2H^+ + 2e^- \rightarrow CH_3OH + H_2O \quad (2)$$

Catalytic oxidation of alternative substrates is also of interest, and MMOH offers many such opportunities including olefin epoxidation, arene hydroxylation, and amine and sulfide oxidation. As mentioned in the

previous section, a challenge is to determine whether catalytic oxidation reactions of this kind bear any similarities to those that occur in the natural systems. One major difficulty in designing such a catalytic system for monooxygenases is the need for a reductant in addition to the substrate (eq 2). In MMOH, oxidation of unsubstituted alkanes requires a high-valent di(μ-oxo)diiron(IV) species, which then converts to the diiron(III) state of the resting enzyme (Scheme 3).[13] In the biological system, further reduction of this diiron(III) species to the diiron(II) reduced state is required in order to close the catalytic cycle. This step involves oxidation of NADH, which binds to a different protein (MMOR), thus avoiding contact with the reactive diiron(IV) intermediate in the hydroxylase. In synthetic model chemistry, however, all components are typically present in solution. Thus, use of a reductant that will not react with oxygenated diiron intermediates presents a challenge. This problem may not arise when mimicking dioxygenase activity, since the reduction step is unnecessary.

Despite the difficulties and challenges just outlined, significant progress has been made in recent years in the field of modeling carboxylate-bridged diiron metalloenzymes, as discussed in the following sections.

3. Diiron(II) Complexes

An attractive way to approach diiron metalloprotein modeling is the synthesis of diiron(II) complexes having the stoichiometry and geometric features of the catalytic core of the protein. In this section, we review diiron(II) complexes with a variety of ligand systems designed to meet these objectives. Figure 2 portrays a variety of carboxylate and N-donor ligands that are cited here as well as their abbreviations; additional abbreviations are supplied in a later section of this review. Occasionally, solvent components such as water, hydroxide, alcohol, THF, or MeCN, as well as counterions, will coordinate to the iron atoms in the complexes obtained. Table 2 summarizes Fe···Fe distances in a variety of diiron compounds in varying oxidation states, and Table 3 provides Mössbauer data. In the following discussion we first review selected diiron(II) complexes obtained from simple carboxylate ligands and/or polydentate amide ligands. We then cover compounds derived from more complicated carboxylate ligands designed to achieve dinuclearity.

3.1. Dinuclear Complexes of Simple Carboxylate Ligands

3.1.1. μ-Formato and μ-Acetato Complexes

Many studies have employed the simplest carboxylate ligands, formate and acetate, to mimic the side chains of aspartate and glutamate residues encountered at the active sites of diiron metalloproteins. With the use of formate ion and the bidentate terminal bis(imidazole) ligand BIPhMe, the triply bridged diiron(II) compound [$Fe_2(\mu$-$O_2CH)_3(O_2CH)$-(BIPhMe)$_2$] was assembled (Figure 3).[36,37] The synthesis from $Fe(O_2CH)_2 \cdot 2H_2O$ and free BIPhMe in methanol afforded crystalline material. An X-ray structure analysis revealed an asymmetric compound, having three bridging carboxylate ligands, two of which are bidentate and the third of which is monodentate. In addition, there is one bidentate BIPhMe ligand bound to each iron(II) center and one terminal monodentate formate unit. One of the iron sites in the resulting complex is coordinatively unsaturated. Exposure of this compound to air resulted in a (μ-oxo)diiron(III) compound,[36] presumably via a bimolecular pathway involving a tetranuclear diiron(II)diiron(III) intermediate (Scheme 4).[38] This mechanism was deduced on the basis of dioxygen uptake experiments, which indicated ca. 0.5 mol of O_2 consumed per mol of (μ-oxo)diiron(III) compound formed, EPR studies revealing the formation of a mixed-valent species, and extensive kinetic data.

Scheme 4

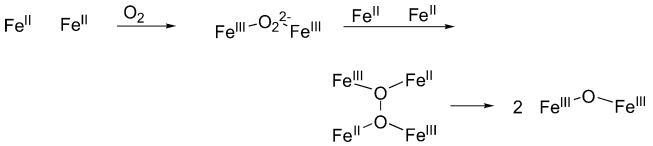

The first synthetic model to mimic the diiron core of the reduced state of Hr is [$Fe_2(\mu$-OH)(μ-OAc)$_2$(Me$_3$-TACN)$_2$]$^+$, illustrated in Figure 4.[39−41] This compound contains two bridging acetate ligands and one terminal tridentate Me$_3$TACN ligand bound to each iron atom. A hydroxo unit also bridges the two iron sites, as observed in deoxy Hr, but the two iron atoms in the model compound are identical, with neither having the empty coordination site available for O_2 binding in the protein (Scheme 1). The Mössbauer spectrum of the diiron(II) model (Table 3) and its magnetic properties are similar to those of reduced Hr. Air oxidation of [$Fe_2(\mu$-OH)(μ-OAc)$_2$(Me$_3$TACN)$_2$]$^+$ generates (μ-oxo)diiron(III) analogues, presumably via a bimolecular mechanism similar to that of Scheme 4.[38] CV studies on the diiron(II) complex in methylene chloride solution indicated the formation of a mixed-valent Fe(II)Fe(III) species.[40] Additional (μ-hydroxo)diiron(II) complexes of Me$_3$TACN ligands with bulkier carboxylate units have been described.[42]

A centrosymmetric cationic complex featuring two bridging acetate ligands and one tripodal nitrogen-based terminal ligand on each iron atom, [$Fe_2(\mu$-

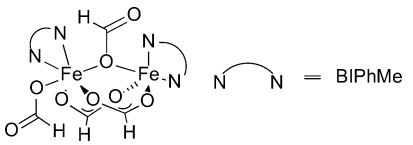

Figure 3. Structure of [$Fe_2(\mu$-$O_2CH)_3(O_2CH)$(BIPhMe)$_2$].[36,37]

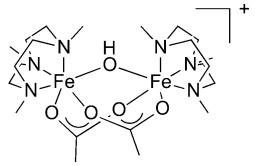

Figure 4. Structure of [$Fe_2(\mu$-OH)(μ-OAc)$_2$-(Me$_3$TACN)$_2$]$^+$.[39−41]

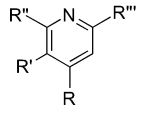

R, R', R'', R''', H: Py
R, *t*-Bu; R', R'', R''', H: *t*-Bu-Py
R, R'', R''', H; R', F: 3-FPy
R, R', H; R'', Me: 2,6-lut
R, R'', H; R', R''', Me: 2,5-lut
R', R''', H; R, R'', Me: 2,4-lut
R, R', R'', H; R''', Me: 2-pic

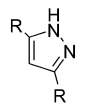

R, Me: Pz^{Me2}

R, H: ImH
R, Me: MeIm
R, Bu: BuIm

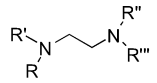

R, R', R'', R''', H: EN
R, R', H; R'', R''', Me: DMEN
R, R', R'', R''', Me: TMEN
R, R', R'', H; R''', CH_2Ph: BZEN
R, R', H; R'', R''', CH_2Ph: DBEN
R, R'', Me; R', R''', CH_2(2-Py): PMEN
R, R'', Et; R', R''', CH_2(2-Py): PEEN
R, CH_2CH_2OH; R', R'', R''', CH_2(2-BzIm): HBIMEN

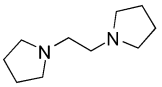

DPE

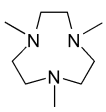

Me_3TACN

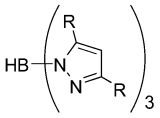

R, H: $HBpz_3$
R, iPr: $HB(3,5\text{-}iPr_2pz)_3$

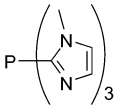

TMIP

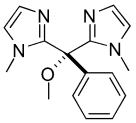

BIPhMe

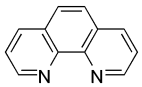

Phen

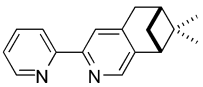

PB

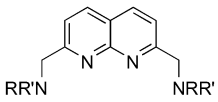

R, R', Et: BEAN
R, R', CH_2Py: BPMAN
R, CH_2Py; R', CH_2CH_2(1-MeIm): BBBAN

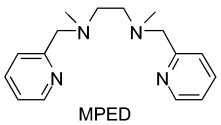

MPED

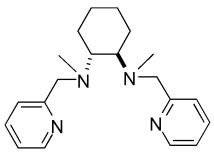

BPMCN

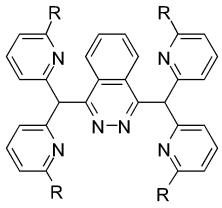

R, H: BDPTZ
R, Ph: Ph_4BDPTZ

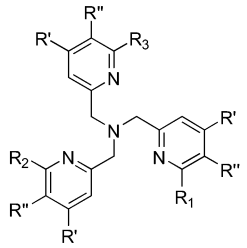

R, R', R'', H: TPA
R', R'', H; R, Me: 6-Me_3-TPA
R, R', H; R'', Me: 5-Me_3-TPA
R', R'', H; R_1, R_2, Me; R_3, Ph: 6,6-Me_2-6-Ph-TPA
R', R'', H; R_1, R_2, H; R_3, Ph: 6-Ph-TPA
R', R'', H; R_1, R_2, H; R_3, Me: 6-Me-TPA
R'', H; R, R', Me: 4,6-Me_6-TPA
R, R', H; R'', Et: 5-Et_3-TPA

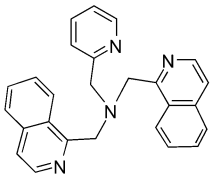

BQPA

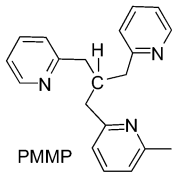

PMMP

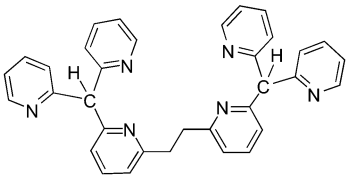

PPE

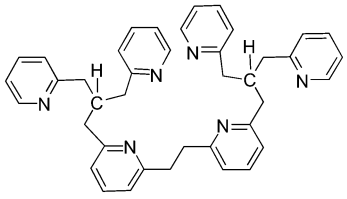

PMPE

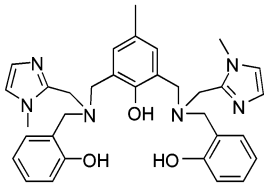

H_3BIOMP

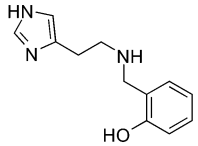

HBHA

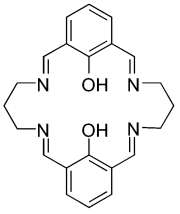

N_4-diphenol macrocycle

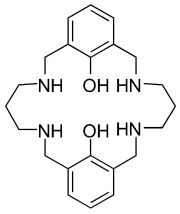

$(NH)_4$-diphenol macrocycle

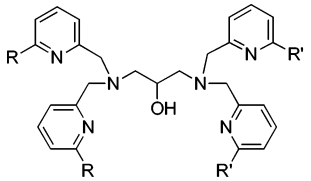

R, R', H: HTPDP
R, H; R', Me: HMe_2TPDP
R, R', Me: HMe_4TPDP
R, R', $NHCOC(Me)_3$: HTPPDO

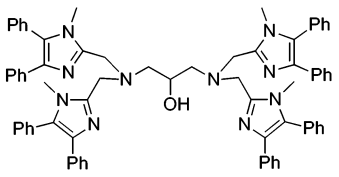

HPh-TIDP

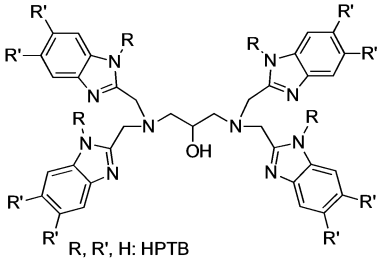

R, R', H: HPTB
R, EtOH; R', H: H-EtOH-HPTB
R, H; R', Me: Me_2HPTB
R', H; R, Et: *N*-Et-HPTB

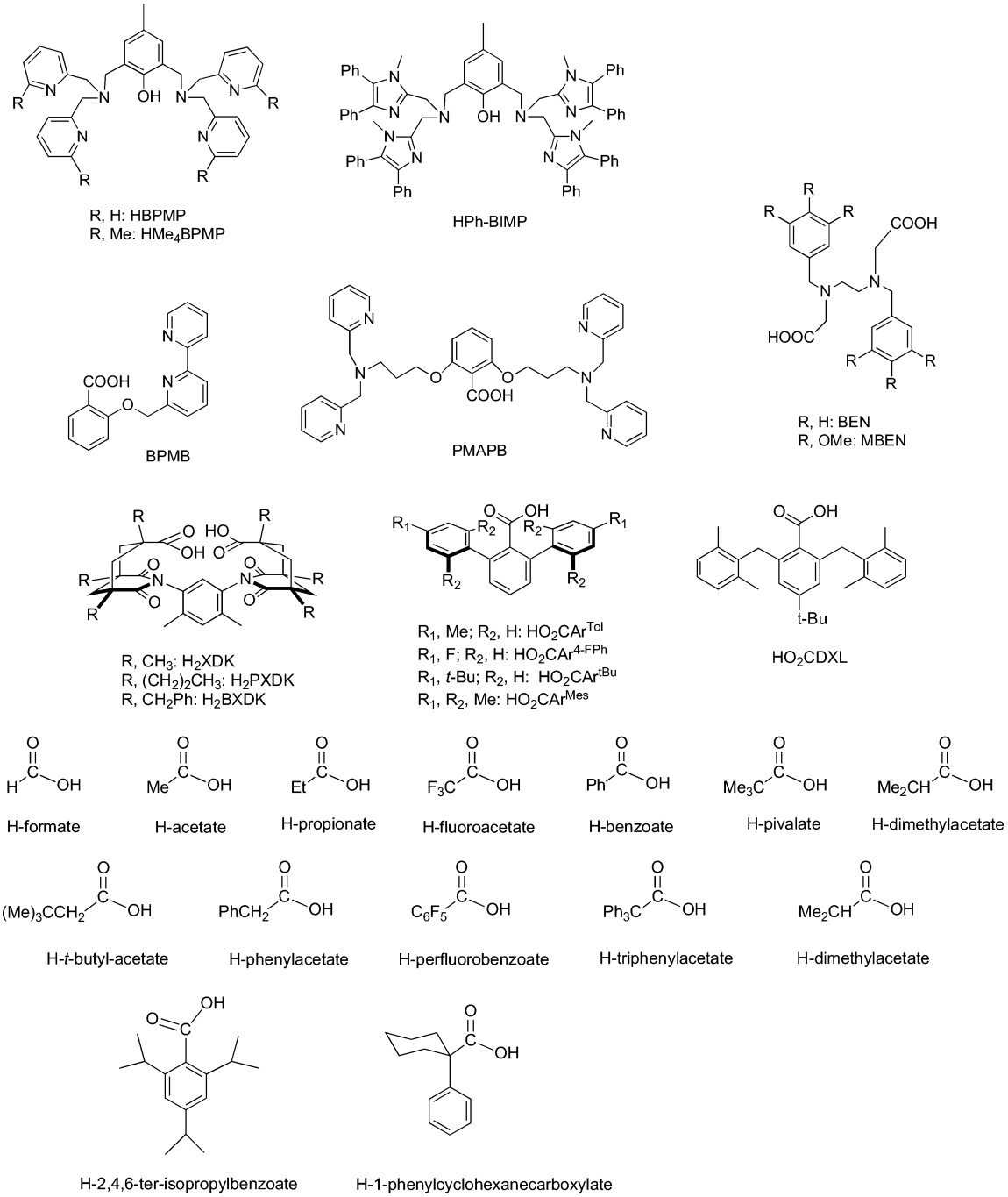

Figure 2. Ligands employed for carboxylate-bridged diiron protein model chemistry.

$OAc)_2(TPA)_2]^{2+}$, is illustrated in Figure 5.[43] The TPA ligands bind in a tetradentate mode, leaving no empty coordination site. Frozen solution Mössbauer and EPR spectroscopic measurements conducted in MeCN indicated a high-spin iron(II) ground state. Exposure of this compound to dioxygen led to the formation of a (μ-oxo)diiron(III) complex having terminal monodentate acetate ligands, possibly by prior decomposition into monomeric species. The tetradentate N_4 ligand MPED (Figure 2) can facilitate the assembly of diiron(II) compounds.[44] The complex $[Fe_2(\mu\text{-}OAc)_2(MPED)_2]^{2+}$ was obtained from the reaction of the ligand with iron(II) acetate and characterized crystallographically. Air oxidation led to the formation of the (μ-oxo)diiron(III) complex $[Fe_2O(\mu\text{-}OAc)(MPED)_2]^{3+}$.

Another asymmetric diiron(II) synthetic model is the anionic complex $[Fe_2(\mu\text{-}H_2O)(\mu\text{-}OAc)_2(OAc)_3(Py)_2]^-$ depicted in Figure 6.[45,46] Its structure features two bridging acetate ligands and three nonbridging ones. A water molecule also links the two iron centers, displacement of which may open a coordination site for O_2 binding. One pyridine ligand, representing the imidazole side chain of histidine residues in the natural systems, is terminally bound to each iron atom. The two pyridine ligands are in a *syn* orientation relative to the iron−iron vector. A related but geometrically different configuration occurs in MMOH (Figure 1) and other diiron proteins, as discussed in section 3.2.3 below. The two monodentate carboxylate ligands, bound to one of the iron atoms, are hydrogen bonded to the bridging water molecule, a common

Table 2. Iron−Iron Distances in Selected Dinuclear Model Compounds

compd	Fe···Fe (Å)	ref	compd	Fe···Fe (Å)	ref
			Fe_2(II)		
$[Fe_2(O_2CH)_2(BIPhMe)_2]$	3.574	36	$[Fe_2(OAc)_2(Ph_4BDPTZ)]^{2+}$	3.479	55
$[Fe_2O(OAc)_5(Py)_2H_2O]^-$	3.577	46	$[Fe_2(OPr)_2(Ph_4BDPTZ)]^{2+}$	3.569	55
$[Fe_2(OH)(OAc)_2(Me_3TACN)_2]^+$	3.32	40	$[Fe_2(O_2CCH_2Ph)_2(Ph_4BDPTZ)]^{2+}$	3.698	55
$[Fe_2(OAc)_2(TPA)_2]^{2+}$	4.288	43	$[Fe_2(OH)(Ph_2DBA)(DPE)_2(OTf)]$	3.267	56b
$[Fe_2(OAc)_2(MPED)_2]^{2+}$	4.382	44	$[Fe_2(ImH)_2(XDK)(OBz)_2(MeOH)]$	3.609	60
$[Fe_2(H_2O)(OAc)_4(TMEN)_2]^{2+}$	3.653	47	$[Fe_2(Py)_2(BXDK)(O_2CPhCy)_2]$	3.565	61
$[Fe_2(H_2O)(O_2CPh)_4(TMEN)_2]^{2+}$	3.620	47	$[Fe_2(Py)_2(O_2CAr^{Tol})_4]$	4.219	65
$[Fe_2(OPr)_2(BPMP)]^+$	3.348	49	$[Fe_2(MeIm)_2(O_2CAr^{Tol})_4]$	4.203	65
$[Fe_2(O_2CPh)(Me_4\text{-}TPDP)(H_2O)]^{2+}$	3.684	52	$[Fe_2(DMEN)_2(O_2CAr^{Tol})_4]$	3.424	64
$[Fe_2(O_2CPh)(Ph\text{-}TIDP)]^{2+}$	3.592	50	$[Fe_2(DMEN)_1(O_2CAr^{Tol})_4]$	3.125	64
$[Fe_2(O_2CPh(p\text{-}Cl))(TPPDO)]^{2+}$	3.732	53	$[Fe_2(DBEN)_2(O_2CAr^{Tol})_4]$	4.360	64
$[Fe_2(O_2CPh)(HTPPDO)]^{3+}$	5.018	53	$[Fe_2(MeCN)_2(O_2CAr^{Mes})_4]$	4.122	72
$[Fe_2(O_2CPhCy)_2(BPMAN)]^{2+}$	3.738	54	$[Fe_2(Piv)_2(OH)(Me_3TACN)_2]^+$	3.424	113
$[Fe_2(OH)(O_2CPhCy)_2(BPMAN)]^{2+}$	3.221	54	$[Fe_2(O_2CPh)(N\text{-}Et\text{-}HPTB)]^{2+}$	3.473	117
$[Fe_2(O_2CPhCy)_3(BEAN)]^+$	2.849	54	$[Fe_2(OH)_2(6\text{-}Me_3\text{-}TPA)_2]^{2+}$	3.187	140
$[Fe_2(OAc)_2(OTf)(BBBAN)]^{2+}$	3.504	54	$[Fe_2(O_2CAr^{Tol})_2(Me_3TACN)_2(MeCN)_2]$	4.713	156
			Fe(II)Fe(III)		
$[Fe_2O(O_2CCPh_3)_2(Me_3TACN)_2]^+$	3.123	42	$[Fe_2(OAc)_2(N_4(ArOH)_2)]^+$	2.741	112
$[Fe_2(OPr)_2(BPMP)]^{2+}$	3.365	49	$[Fe_2(OH)(Piv)_2(Me_3TACN)_2]^{2+}$	3.400	114
$[Fe_2(O^iPr)_2(O_2CAr^{Mes})_3]$	2.624 2.749	71	$[Fe_2O(Piv)_2(Me_3TACN)_2]^+$	3.155	113
			Fe_2(III)		
$[Fe_2(O)_2(6\text{-}Me_3\text{-}TPA)_2]^{2+}$	2.716	102	$[Fe_2O(Piv)_2(Me_3TACN)_2]^{2+}$	3.123	114
$[Fe_2O(O_2CH)_2(BIPhMe)_2]$	3.211	36	$[Fe_2O(OH)(6\text{-}Me_3\text{-}TPA)_2]^{3+}$	2.948	103
$[Fe_2O(OAc)_2(Me_3TACN)_2]^{2+}$	3.12	40	$[Fe_2(O)(OH)(H_2O)(5\text{-}Et_3\text{-}TPA)_2]^{3+}$	3.346	132b
$[Fe_2O(HBpz_3)_2(OAc)_2]$	3.146	90	$[Fe_2O(OH)(BQPA)_2]^{3+}$	2.89	101
$[Fe_2O(TMIP)_2(OAc)_2]^{2+}$	3.158	92	$[Fe_2O(OH)(PEEN)_2]^{3+}$	2.84	101
$[Fe_2O(PMPE)_2(OAc)_2]^{2+}$	3.142	93	$[Fe_2O(H_2O)(OH)(TPA)_2]^{3+}$	3.389	132a
$[Fe_2O(XDK)_2(OAc)_2(MeOH)_5(H_2O)]^{2+}$	3.226	94	$[Fe_2(\mu\text{-}OH)(\mu\text{-}O_2CAr^{Tol})$-(BDPTZ)(MeCN)(OTf)]$^+$	3.267	74
$[Fe_2O(BIOMP)_2(OAc)_2]^+$	3.567	100	$[Fe_2(OH)_2(Py)_2(O_2CAr^{Tol})_4]$	2.832	63
$[Fe_2O(BHA)_2(OCH_3)_2(OAc)]^+$	3.105	99	$[Fe_2(OH)_2(t\text{-}Bu\text{-}Py)_2(O_2CAr^{Tol})_4]$	2.884	63
$[Fe_2O(O_2CH)(MeIm)_8]^{3+}$	3.285	104	$[Fe_2(OH)_2(DBEN)(BZEN)(O_2CAr^{Tol})_4]$	2.979	64
$[Fe_2O(OAc)(MeIm)_8]^{3+}$	3.29	104			
			Peroxo		
$[Fe_2(O-O)(N\text{-}Et\text{-}HPTB)(Ph_3PO)_2]^{3+}$	3.462	118	$[Fe_2(O-O)(O_2CCH_2Ph)_2(HB(3,5\text{-}^iPr_2pz)_3)_2]$	4.000	124
$[Fe_2(O-O)(O_2CPh)(Ph\text{-}BIMP)]^{2+}$	3.327	122	$[Fe_2(O-O)(O)(6\text{-}Me_3\text{-}TPA)_2]^{2+\,a}$	3.14[b]	135
			Fe_2(III,IV)		
$[Fe_2(O)_2(5\text{-}Me_3\text{-}TPA)_2]^{3+\,a}$	2.89[b]	132b	$Fe_2(O)_2(5\text{-}Et_3\text{-}TPA)_2]^{3+}$	2.683	134
			Fe_2(IV)		
$[Fe_2(O)_2(BPMCN)_2]^{4+\,a}$	2.81[b]	141			

[a] Postulated. [b] Data obtained from EXAFS measurements; otherwise from X-ray crystallography.

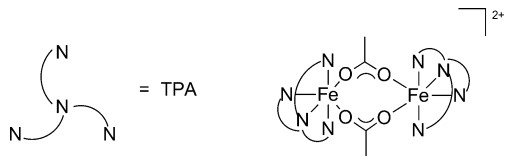

Figure 5. Structure of $[Fe_2(\mu\text{-}OAc)_2(TPA)_2]^{2+}$.[43]

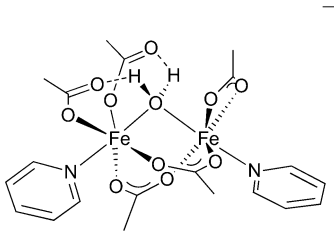

Figure 6. Structure of $[Fe_2(\mu\text{-}H_2O)(\mu\text{-}OAc)_2(OAc)_3(Py)_2]^-$.[45,46]

feature in dimetallic μ-aqua complexes. The appearance of one sharp quadrupole doublet in the solid state Mössbauer spectrum of this compound (Table 3), which is unlikely to result from such an asymmetric structure, implies that this complex adopts a different geometry in solution. Magnetization studies indicated that the compound is weakly antiferromagnetically coupled in the solid state, and reactions with dioxygen and H_2O_2 lead to higher nuclearity complexes.

3.1.2. Complexes of Polyamine and Polypyridine Ligands

The μ-aqua complexes $[Fe_2(\mu\text{-}H_2O)(\mu\text{-}O_2CR)_2(O_2CR)_2(TMEN)_2]$ (R = Me or Ph) feature two TMEN (Figure 2) ligands bound in a bidentate fashion.[39,47] Both compounds exhibit hydrogen bonding interactions between the bridging water molecule and the nonbridging monodentate carboxylate units. The Mössbauer spectra (Table 3) and magnetic interactions are consistent with high-spin diiron(II) complexes.

Complexes having a non-water-derived single atom bridge in addition to bridging carboxylate units were synthesized by using dinucleating polydentate ligands such as BPMP (Figure 2).[48,49] A diiron(II) compound having a (μ-phenoxo)bis(μ-carboxylato) core was obtained with the ligand BPMP (Figure 2). Its crystal

Table 3. Mössbauer Parameters of Selected Diiron Model Compounds

compd	T, K	δ, mm s^{-1}	ΔE_Q, mm s^{-1}	ref	compd	T, K	δ, mm s^{-1}	ΔE_Q, mm s^{-1}	ref
					Fe_2(II)				
$[Fe_2(O_2CH)_2(BIPhMe)_2]$	4.2	1.26	2.56	36	$[Fe_2(OAc)_2(Ph_4BDPTZ)]^{2+}$	4.2	1.17	2.25	55
		1.25	3.30				1.14	2.78	
$[Fe_2O(OAc)_5(Py)_2H_2O]^-$	125	1.30	2.00	46	$[Fe_2(OPr)_2(Ph_4BDPTZ)]^{2+}$	4.2	1.14	2.14	55
$[Fe_2(OH)(OAc)_2(Me_3TACN)_2]^+$	4.2	1.16	2.83	40			1.15	2.64	
$[Fe_2(H_2O)(O_2CPh)_4(TMEN)_2]$	4.2	1.27	2.75	47	$[Fe_2(O_2CCH_2Ph)_2(Ph_4BDPTZ)]^{2+}$	4.2	1.14	2.49	55
$[Fe_2(H_2O)(OAc)_4(TMEN)_2]$	4.2	1.25	3.11	47			1.17	2.85	
		1.26	2.70		$[Fe_2(OH)(Ph_2DBA)(DPE)_2(OTf)]$	4.2	1.23	2.79	56b
$[Fe_2(OAc)_2(TPA)_2]^{2+}$	4.2	1.12	3.33	43	$[Fe_2(ImH)_2(XDK)(O_2CPh)_2$-(MeOH)]	4	1.35	3.04	60
$[Fe_2(OPr)_2(BPMP)]^+$	55	1.20	2.72	49			1.12	2.83	
$[Fe_2(O_2CPhCy)_2(BPMAN)]^{2+}$	4.2	1.18	3.01	54	$[Fe_2(Py)_2(BXDK)(O_2CPhCy)_2]$	77	1.06	2.56	61
$[Fe_2(OH)(O_2CPhCy)_2$-(BPMAN)]$^{2+}$	4.2	1.13	2.66	54			1.28	3.01	
		1.18	2.93		$[Fe_2(Py)_2(O_2CAr^{Tol})_4]$	4.2	1.19	3.02	65
$[Fe_2(O_2CPhCy)_3(BEAN)]^+$	4.2	1.05	1.95	54	$[Fe_2(MeIm)_2(O_2CAr^{Tol})_4]$	4.2	1.19	3.01	65
		1.08	2.79		$[Fe_2(DBEN)_2(O_2CAr^{Tol})_4]$	4.2	1.19	2.90	64
$[Fe_2(OAc)_2(OTf)(BBBAN)]^{2+}$	4.2	1.20	3.28	54	$[Fe_2(py)_2(O_2CAr^{mes})_4]$	4.2	1.14	3.23	73
		1.24	3.03		$[Fe_2(O_2CPh)(N\text{-}Et\text{-}HPTB)]^{2+}$	298	1.07	3.13	117
					Fe(II)Fe(III)				
$[Fe_2O(O_2CCPh_3)_2(Me_3TACN)_2]^+$	4.2	1.09	2.45	42			0.94	2.6	
		0.6	2.35		$[Fe_2(OAc)_2(N_4$-diphenol-macrocycle)]$^+$	293	0.71	1.89	112
$[Fe_2(OPr)_2(BPMP)]^{2+}$	55	0.48	0.50	49	$[Fe_2(OAc)_2(H_2O)((NH)_4$-diphenol-macrocycle)]$^+$	293	0.95	3.17	112
		1.13	2.69				0.50	0.71	
$[Fe_2(O^iPr)_2(O_2CAr^{Mes})_3]$	4.2	a 0.76	2.0	71	$[Fe_2(OH)(Piv)_2(Me_3TACN)_2]^{2+}$	300	0.80	1.12	114
		b 0.59	1.6				0.55	0.68	
					Fe_2(III)				
$[Fe_2(O)_2(6\text{-}Me_3\text{-}TPA)_2]^{2+}$	4.2	0.50	1.93	102	$[Fe_2O(Piv)_2(Me_3TACN)_2]^{2+}$	4.2	0.48	1.54	114
$[Fe_2O(OAc)_2(Me_3TACN)_2]^{2+}$	4.2	0.47	1.50	40	$[Fe_2O(O_2CAr^{Tol})_2(Me_3TACN)_2]$	4.2	0.50	1.84	156
$[Fe_2O(HBpz_3)_2(OAc)_2]$	4.2	0.52	1.60	90	$[Fe_2O(OH)(6\text{-}Me_3\text{-}TPA)_2]^{3+}$	4.2	0.51	1.66	103
		0.52	0.71		$[Fe_2O(OH)(5\text{-}Et_3\text{-}TPA)_2]^{3+}$	4.2	0.45	−1.70	132b
$[Fe_2O(TMIP)_2(OAc)_2]^{2+}$	4.2	0.52	1.65	92			0.45	−0.99	
$[Fe_2O(PMPE)_2(OAc)_2]^{2+}$	4.2	0.52	1.79	93	$[Fe_2(OH)_2(t\text{-}Bu\text{-}Py)_2(O_2CAr^{Tol})_4]$	4.2	0.49	1.01	63
$[Fe_2O(BIOMP)_2(OAc)_2]^+$	295	0.41	1.08	100	$[Fe_2(OH)_2(DBEN)(BZEN)$-$(O_2CAr^{Tol})_4]$	4.2	0.48	0.61	64
$[Fe_2O(BHA)_2(OCH_3)_2(OAc)]^+$	115	0.47	0.80	99					
					Peroxo				
$[Fe_2(O-O)(O_2CPh)$-(Ph-BIMP)]$^{2+}$	77	0.58	0.74	122			0.63	1.20	
		0.65	1.70		$[Fe_2(O-O)(Py)_2(O_2CDXL)_4]^a$	4.2	0.65	1.27	73
$[Fe_2(O-O)(O_2CCH_2Ph)_2$-$(HB(3,5\text{-}^iPr_2pz)_3)_2]$	4.2	0.66	1.40	124			0.52	0.71	
$[Fe_2O(O-O)(6\text{-}Me_3\text{-}TPA)_2]^{2+\,a}$	4.2	0.54	1.68	135	$[Fe_2O(O-O)(OAc)(PPE)]^{+\,a}$	4.2	0.53	1.67	129
$[Fe_2(O-O)(Py)_2(BXDK)$-$(O_2CPhCy)_2]^a$	77	0.47	0.88	61	$[Fe_2O(O-O)(H_2O)_2(PB)_4{}^{4+}]^a$	4.2	0.49	0.62	130
					Fe_2(III,IV)				
$[Fe_2(O)_2(5\text{-}Me_3\text{-}TPA)_2]^{3+a}$	4.2	0.14	0.49	132b	$[Fe_2(O)_2(6\text{-}Me\text{-}TPA)]^+$	150	0.48	1.6	133
							0.08	0.5	
					Fe_2(IV)				
$[Fe_2(O)_2(BPMCN)_2]^{4+\,a}$	4.2	0.10	1.75	141					

[a] Characterized spectroscopically rather than crystallographically.

structure and Mössbauer properties indicated symmetrical high-spin iron(II) centers.

Various other alkoxo-type dinucleating ligands were employed to assemble diiron(II) compounds as possible mimics for diiron metalloenzymes, including HTPDP, HPTB, and others (Figure 2).[50−52] For example, the ligand HTPPDO (Figure 2) generates a (μ-alkoxo)(μ-carboxylato) compound $[Fe_2(TPPDO)\{\mu$-$O_2CC_6H_4(p\text{-}Cl)\}]^{2+}$.[53] The crystal structure revealed two symmetrical iron centers, bridged by one benzoate ligand and the alkoxide group, with both iron atoms being seven-coordinate. Other diiron(II) complexes of this family, such as $[Fe_2(HTPPDO)$-$(\mu\text{-}O_2CPh)]^{2+}$, exhibit asymmetric structures. In these the alkoxide group is bound to only one iron atom, leaving the other six-coordinate.

A series of (μ-carboxylato)(μ-1,8-naphthyridine)-diiron(II) complexes were prepared by employing the dinucleating ligands BPMAN, BEAN, and BBBAN (Figure 2).[54] These complexes were studied by CV and Mössbauer spectroscopy (Table 3). The compound $[Fe_2(BPMAN)(\mu\text{-}O_2CPhCy)_2]^{2+}$ (Figure 7) exhibits two reversible one-electron redox waves, assigned to the Fe(III)Fe(II)/Fe(II)Fe(II) and Fe(III)Fe(III)/Fe(III)-Fe(II) couples. This result suggests that diiron(II) sites bridged by carboxylate units in biology might

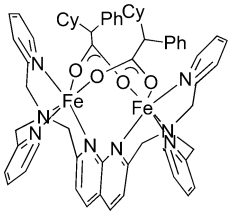

Figure 7. Structure of $[Fe_2(BPMAN)(\mu\text{-}O_2CPhCy)_2]^{2+}$.[54]

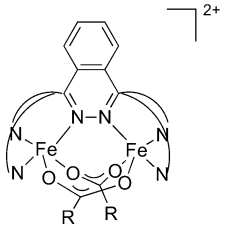

Figure 8. Structure of $[Fe_2(\mu\text{-}O_2CR)_2(Ph_4BDPTZ)_2]^{2+}$.[55]

serve as one- or two-electron donors without a significant change in geometry.

Another related ligand system used to synthesize diiron compounds is derived from phthalazine (Figure 2).[55] Complexes of the type $[Fe_2(\mu\text{-}O_2CR)_2(Ph_4BDPTZ)_2]^{2+}$ (Figure 8) (R = Me, Et, CH_2Ph, ^tBu) were prepared, where the pendant pyridine arms coordinate to the metal atoms, providing additional stability to the coordinatively unsaturated diiron(II) center. The phenyl rings form a hydrophobic pocket in which additional ligands can be accommodated and block possible formation of tetranuclear species, which occurs in the BDPTZ analogues. The increased steric bulk also shifts the carboxylate binding from a *syn, anti* to a *syn, syn* mode. Mössbauer studies (Table 3) are consistent with the formation of relatively symmetric complexes.

3.2. Complexes of Dinucleating Carboxylate Ligands

3.2.1. Complexes of the Ligands DBA and XDK and Its Analogues

Interesting models of Hr were obtained from the ligand Ph_4DBA (Figure 2).[56] For example, the compound $[Fe_2(OH)(Ph_2DBA)(DPE)_2(OTf)]$ was found to contain the asymmetric coordination environment of deoxyHr according to X-ray crystallography and Mössbauer studies (Table 3). Oxygenation of this compound with O_2 yields a μ-oxo species, a model for oxyHr.

XDK (Figure 2)[57] and its analogues have been studied extensively as dinucleating ligands to afford coordinatively unsaturated diiron(II) complexes. In the compound $[Fe_2(\mu\text{-}H_2O)(\mu\text{-}O_2CCF_3)_2(\mu\text{-XDK})(TMEN)_2]$ (Figure 9a),[58] the XDK ligand is bound to both iron atoms via its two carboxylate units, which are also hydrogen bonded to a bridging water molecule. One TMEN ligand coordinates to each iron center in a bidentate mode. With the water molecule present, the compound is coordinatively saturated. This compound and its analogues may be obtained by exchange of the $CF_3CO_2^-$ ligands in a complex of the type $[Fe_2(\mu\text{-}H_2O)(\mu\text{-}O_2CCF_3)_2(O_2CCF_3)_2(TMEN)_2]$ with the XDK derivative.

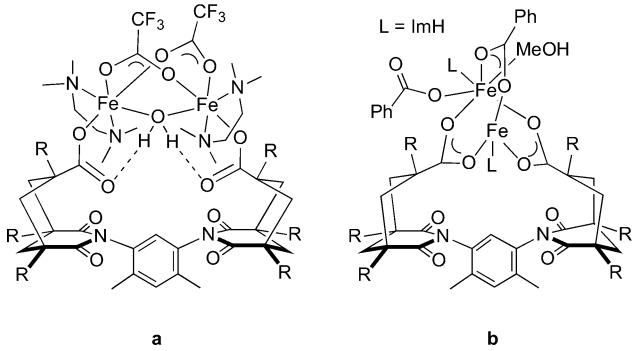

Figure 9. Structure of complexes containing the ligand XDK: (a) $[Fe_2(\mu\text{-}H_2O)(\mu\text{-}O_2CCF_3)_2(\mu\text{-XDK})(TMEN)_2$;[58] (b) $[Fe_2(\mu\text{-}O_2CPh)(XDK)(ImH)_2(O_2CPh)(MeOH)]$.[59,60]

Another member of this family is $[Fe_2(\mu\text{-}O_2CPh)(XDK)(ImH)_2(O_2CPh)(MeOH)]$ (Figure 9b), featuring monodentate terminal imidazole ligands.[59,60] One iron atom in this complex, as observed from its X-ray structure, has a bound methanol solvent molecule and is thus six-coordinate, whereas the other iron atom is pentacoordinate and coordinatively unsaturated. This diiron(II) compound was the first to be reported having four carboxylate units, two monodentate terminal nitrogen ligands, and a solvent molecule, similar to the composition of the reduced state of MMOH. Several analogues were described, with a variety of other bridging units, including halides, triflate, or carboxylate ions.[59−61] Magnetic measurements indicated weak antiferromagnetic coupling, and the frozen solution Mössbauer spectrum reflected the presence of two inequivalent iron centers (Table 3), demonstrating that similar structures may be present in the solid and solution states.

3.2.2. Complexes of m-Terphenyl Carboxylate Ligands

Bulky ligands of the *m*-terphenyl carboxylate family (Figure 2) have been used to prepare coordinatively unsaturated dinuclear iron(II) complexes in the absence of chelating N-donors.[62−69] In addition to supporting dinuclearity, these bulky ligands provide a hydrophobic shield around the diiron core, which is an advantage when attempting to model the chemistry of the enzyme active sites. Complexes in this family generally contain four carboxylate ligands and two additional coordinating groups, such as THF, pyridine, or MeIm. They are thus similar in stoichiometry to the active sites of non-heme diiron metalloenzymes in their reduced state, a typical complex having the formula $[Fe_2(\mu\text{-}O_2CAr)_2(O_2CAr)_2(L)_2]$. These complexes exist in solution as an equilibrium between quadruply bridged "paddlewheel" and doubly bridged "windmill" structures, as illustrated in Scheme 5. Steric interactions between the carboxylate ligands and/or the terminal groups determine which is the

Scheme 5

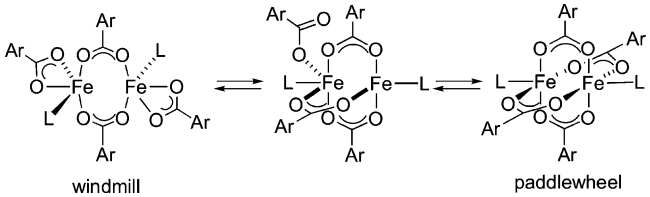

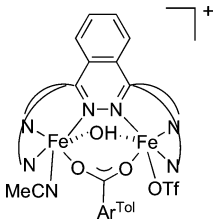

Figure 10. Structure of $[Fe_2(\mu\text{-OH})(\mu\text{-}O_2CAr^{Tol})(BDPTX)(MeCN(OTf)]^+$.[74]

major species in solution. Crystal structures of complexes having the windmill structure revealed a relatively long Fe···Fe distance, of 3.96−4.22 Å (Table 2), with the terminal carboxylate bound in either a monodentate or bidentate mode. By contrast, complexes exhibiting the paddlewheel structure feature a shorter Fe···Fe distance of 2.73−2.85 Å, as expected due to the four bridging carboxylate ligands. The Mössbauer (Table 3) and magnetic properties of these complexes are comparable to those of other high-spin diiron(II) compounds. When employing the more crowded carboxylate ligand $^-O_2CAr^{Mes}$ (Figure 2), a sterically encumbered dinuclear complex can be obtained with MeCN as the terminal ligand.[70−72] Bulky N-donor ligands such as py or MeIm lead to mononuclear complexes with this carboxylate. To overcome the difficulty and achieve the advantages of the related *m*-terphenyl carboxylate ligands, an additional methylene unit was introduced between the aryl ring and the O_2C- unit ($^-O_2CDXL$, Figure 2).[73] This carboxylate ligand facilitated formation of several diiron(II) complexes having paddleweel structures, with a variety of terminal N-donor ligands.

^{19}F NMR studies of complexes containing *p*-fluorophenyl substituted carboxylate ligands ($^-O_2CAr^{4\text{-}FPh}$, Figure 2), revealed the interconversion of the windmill and paddlewheel structures to involve carboxylate shifts, with the paddlewheel structure being preferred at low temperature (Scheme 5).[65] Such a carboxylate shift process may assist in opening a coordination site for dioxygen binding, as occurs in the natural systems during catalysis.[1,33,34]

The bulky $^-O_2CAr^{Tol}$ ligand has also been employed in combination with the pyridine-containing ligand BDPTZ (Figure 2) to prepare $[Fe_2(\mu\text{-OH})(\mu\text{-}O_2CAr^{Tol})(BDPTZ)(MeCN)(OTf)]^+$ (Figure 10).[74] This compound converts to the (μ-oxo)diiron(III) analogue upon exposure to dioxygen.

3.2.3. Syn N-Donor Ligands

It was recently revealed by density functional theoretical calculations that the *syn* disposition of the imidazole groups relative to the Fe−Fe vector in the active site of MMOH[13] (Figure 1) facilitates C−H bond activation by intermediate Q.[75] No complex has yet been reported that replicates this important structural feature by enforcing *syn* stereochemistry using a suitable dinucleating ligand. Recently, we designed and prepared a family of 1,2-dipropargylbenzene ligands that afford the desired *syn*-N−N structure.[76] An example of such a complex is the diiron(II) species $[Fe_2(\mu\text{-OH})(\mu\text{-}O_2CAr^{Tol})(O_2CAr^{Tol})_2(L)(H_2O)]$ (Figure 11), which was crystallographically characterized. This compound has several interesting

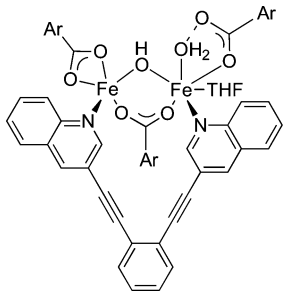

Figure 11. Structure of $[Fe_2(\mu\text{-OH})(\mu\text{-}O_2CAr^{Tol})(O_2CAr^{Tol})_2(L)(H_2O)]$ exhibiting two *syn*-N-donor ligands.[76b]

features; it exhibits *syn* coordination of the N-donor groups relative to the diiron vector. It is asymmetric, similar to the active site of MMOH, and it contains a terminal water molecule, again as in the enzyme MMOH.[13] We have not yet fully explored its reactivity, but investigations of this and related compounds, including ones derived from bis(N-donor)bis(carboxylate) ligands,[76] are currently in progress.

3.3. Protein Design: Four Helix Bundle Models

A different approach to modeling enzyme active sites is to synthesize small peptides with a defined amino acid sequence having sufficient information for proper protein folding.[77−80] Such a "de novo" protein design methodology affords models that are simpler and smaller than the full protein and have the potential to exhibit similar functional properties.

De novo design of diiron-based protein model systems has focused on four-helix bundles, modeled after the structures of diiron proteins such as Hr and MMOH.[81,82] In several of these diiron proteins there is a dimeric helix−loop−helix motif that generates the bundle. Each unit provides two glutamate residues, one from each helix, and a single histidine residue. A corresponding four-helix bundle diiron model in this class, DF1, was designed and synthesized. It exhibits the dimeric helix−loop−helix motif, providing the requisite four glutamate and two histidine residues needed to recapitulate the active site.[83−85] The synthetic protein binds zinc(II) in a dimeric form, the crystal structure of which confirms the positions of two bridging glutamate ligands, two chelating ones, and two monodentate histidine residues. The metal center has a Zn···Zn distance of 3.9 Å. The geometry closely reproduces that of the diiron enzymes. The solid-state structure of the dizinc complex also resembles the solution structure of the apo bundle, which was determined by NMR spectroscopy. DF1 also binds manganese(II), cobalt(II), and iron(II), and may thus serve as a model for diiron metalloenzymes.

The DF1 peptide model is insoluble in aqueous buffer solution and has two hydrophobic side chain units blocking access to the active site. An improved model, DF2, was therefore designed.[86,87] It is highly water soluble and binds metal ions reversibly. The dimetallic center in the metal-bound protein is accessible to dioxygen, as suggested by the crystal structure of the dimanganese form (Figure 12), which reveals a geometry similar to that of dizinc-DF1. Morover, the iron-bound DF2 exhibits ferroxidase

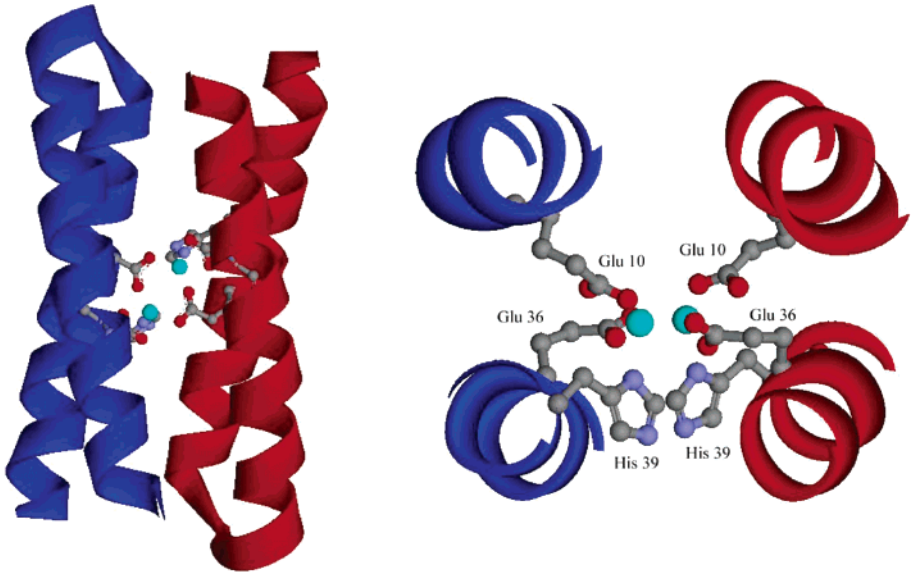

Figure 12. Structure of the dimanganese form of DF2. At the right is a perpendicular view, in which the helices are omitted to reveal the dimetal binding site; the Mn···Mn distance is 3.64 Å.[86,87]

Table 4. Resonance Raman Data of Selected Diiron Model Compounds

compd	vibration	signal, cm^{-1}	signal shift upon ^{18}O labeling	ref
$[Fe_2O(O_2CH)_2(BIPhMe)_2]$	$\nu(FeOFe)_s$	520	502	36
$[Fe_2O(HBpz_3)_2(OAc)_2]$	$\nu(FeOFe)_s$	528	511	90
$[Fe_2O(Piv)_2(Me_3TACN)_2]^+$	$\nu(FeOFe)_{as}$	711	675	113
$[Fe_2O(OH)(6\text{-}Me_3\text{-}TPA)_2]^{3+}$	$\nu(FeOFe)_s$	591	564	103
$[Fe_2O(OH)(6\text{-}Me_3\text{-}TPA)_2]^{3+}$	$\nu(FeOFe)_{as}$	675, 666	645, 634	103
$[Fe_2O(OH)(BQPA)_2]^{3+}$	$\nu(FeOFe)_s$	600	575	101
$[Fe_2O(OH)(BQPA)_2]^{3+}$	$\nu(FeOFe)_{as}$	668	632	101
$[Fe_2O(OH)(PEEN)_2]^{3+}$	$\nu(FeOFe)_s$	596	567	101
$[Fe_2O(OH)(PEEN)_2]^{3+}$	$\nu(FeOH)_{as}$	504	497	101
$[Fe_2O(OH)(5\text{-}Me_3\text{-}TPA)_2]^{3+}$	$\nu(FeOFe)_s$	458	446	132b
$[Fe(O-O)(O_2CCH_2Ph)(HB(3,5\text{-}^iPr_2pz)_3)]$	$\nu(O-O)$	888	842	124
$[Fe_2O(O-O)(OAc)(PPE)]^+$	$\nu(O-O)$	816	771	129
$[Fe_2O(O-O)(H_2O)_2(PB)_4]^{4+}$	$\nu(O-O)$	867	819	130
$[Fe_2O(O_2H)(H_2O)_2(PB)_4]^{4+}$		806	762	
$[Fe_2O(O-O)(6\text{-}Me_3\text{-}TPA)_2]^{2+}$	$\nu(O-O)$	848	802	135
$[Fe_2(O-O)(O_2CPh)(Me_4\text{-}TPDP)(H_2O)]^{2+}$	$\nu(Fe-O)$	486, 450	479, 442	52
$[Fe_2(O-O)(O_2CPh)(Me_4\text{-}TPDP)(H_2O)]^{2+}$	$\nu(O-O)$	918, 891	889, 857	52
$[Fe_2(O-O)(O_2CPh)(HTPPDO)]^{3+}$	$\nu(O-O)$	873, 887	825, 839	53
$[Fe_2(O-O)(Py)_2(BXDK)(O_2CPhCy)_2]$	$\nu(O-O)$	861	811	61
$[Fe_2(O-O)(MeCN)_2(O_2CDXL)_4]$	$\nu(O-O)$	885	871	72
$[Fe_2(O-O)(Py)_2(O_2CAr^{Mes})_4]$	$\nu(O-O)$	822	779	73
$[Fe_2(O-O)(OH)_2(6\text{-}Me_3\text{-}TPA)_2]^{2+}$	$\nu(O-O)$	848	802	140
$[Fe_2(O)_2(5\text{-}Me_3\text{-}TPA)_2]^{3+}$	$\nu(Fe-O)$	676, 656	634	132b
$[Fe_2(O)_2(BPMCN)_2]^{4+}$	$\nu(Fe-O)$	686, 679, 653	658, 627	141

activity. Addition of O_2 generates the (μ-oxo)diiron(III) core with absorption bands at 300−350 and 400−700 nm. The diiron(III) form appears to bind azide and acetate anions, as suggested by spectroscopic changes that occur upon their addition. This result implies that the coordinatively saturated diiron center may alter coordination modes, undergoing carboxylate shifts, in order to bind the additional anion successfully, as is the case with natural metalloenzymes.[33]

A related heterotetrameric four-helix bundle protein, $A_aA_bB_2$, has also been synthesized, which self-assembles into the desired tertiary structure through noncovalent interactions.[88] Upon addition of iron(II) and dioxygen, a strong absorption band appears at 625 nm ($\epsilon = 1000\ M^{-1}\ cm^{-1}$) in the spectrum, which resembles those of diiron(III) peroxo intermediates in natural metalloenzymes and their synthetic models (Table 5, vide infra).

4. Diiron(III) Complexes

Diiron(III) complexes in this class are often obtained from the reaction of iron(II) precursors with an oxidant. Alternatively, diiron(III) complexes as models for the oxidized state of the metalloprotein can be generated directly from an iron(III) precursor, as described below. Most common are complexes having an oxo bridge, which appears in Hr and RNR (Schemes 1 and 2).[11,89] Tables 2−5 summarize Fe···Fe distances, Mössbauer parameters, resonance Raman data, and electronic absorption band maxima, respectively.

Table 5. Electronic Absorption of Selected Intermediates and Structural Motifs

compd	structural motif	absorption, nm	ϵ	ref
$[Fe_2(O-O)(O_2CPh)(Me_4\text{-}TPDP)(H_2O)]^{2+}$	μ-1,2-peroxo	616	2000	52
$[Fe_2(O-O)(O_2CPh(p\text{-}Cl))(TPPDO)]^{2+}$	μ-1,2-peroxo	~550	~1500	53
$[Fe_2(O-O)(O_2CPh)(HTPPDO)]^{3+}$	μ-1,2-peroxo	~580	~1300	53
$[Fe_2(O-O)(ImH)_2(XDK)(O_2CPh)_2(MeOH)]$	μ-1,2-peroxo	660	170[a]	60
$[Fe_2(O-O)(Py)_2(BXDK)(O_2CPhCy)_2]$	μ-1,2-peroxo	~580	~1200	61
$[Fe_2(O-O)(MeCN)_2(O_2CAr^{Mes})_4]$	μ-1,2-peroxo	540	2300	72
$[Fe_2(O-O)(Py)_2(O_2CDXL)_4]$	peroxo	500	1000	73
$[Fe_2(O-O)(O_2CPh)(N\text{-}Et\text{-}HPTB)]^{2+}$	μ-1,2-peroxo	588	1500	117
$[Fe_2(O-O)(O_2CPh)(Ph\text{-}BIMP)]^{2+}$	μ-1,2-peroxo	500−800 br	~1700	122
$[Fe(O-O)(O_2CPh)(HB(3,5\text{-}^iPr_2pz)_3)]$	μ-1,2-peroxo	682	3450	123
$[Fe(O-O)(O_2CCH_2Ph)(HB(3,5\text{-}^iPr_2pz)_3)]$	μ-1,2-peroxo	694	2650	124
$[Fe_2O(O-O)(6\text{-}Me_3\text{-}TPA)_2]^{2+}$	μ-1,2-peroxo	494	1100	135
		648	1200	
$[Fe_2O(O-O)(OAc)(PPE)]^{+}$	μ-1,2-peroxo	510	1300	129
		605	1310	
$[Fe_2O(O-O)(H_2O)_2(PB)_4]^{4+}/[Fe_2O(O_2H)(H_2O)_2(PB)_4]^{4+}$	μ-1,2-peroxo O−O−H	680	2000	130
$[Fe_2(O-O)(OH)_2(6\text{-}Me_3\text{-}TPA)_2]^{2+}$	μ-1,2-peroxo	490	1100	140
		640	1100	
$[Fe_2O(OH)(PEEN)_2]^{3+}$	μ-hydroxo-μ-oxo	378	4800	101
		430	2000	
		475	650	
		510	560	
		558	800	
		790	80	
$[Fe_2O(OH)(6\text{-}Me_3\text{-}TPA)_2]^{3+}$	μ-hydroxo-μ-oxo	340	5000	103
		396	4700	
		550	780	
		800	70	
$[Fe_2O(OH)(BQPA)_2]^{3+}$	μ-hydroxo-μ-oxo	308	17 000	101
		396	4500	
		554	790	
		800	60	
$[Fe_2(O)_2(6\text{-}Me_3\text{-}TPA)_2]^{2+}$	bis(μ-oxo)	320	4200	102
		375	2000	
		470	560	
		760	80	
$[Fe_2(O)_2(5\text{-}Me_3\text{-}TPA)_2]^{3+}$	di(μ-oxo)	336	7900	132b
		616	5200	
$[Fe_2(O)_2(6\text{-}Me\text{-}TPA)_2]^{3+}$	di(μ-oxo)	350	8000	133
$[Fe_2(O)_2(BPMCN)_2]^{4+}$	di(μ-oxo)	656	~4000	141
		845	~3500	

[a] Kinetically detected intermediate, not fully formed.

4.1. Direct Assembly of Diiron(III) Complexes from Ferric Salts and Appropriate Ligands

At the active site of several metalloproteins in their resting state is a (μ-oxo)(μ-carboxylato)diiron(III) unit.[11] The first model compounds having this feature were $[Fe_2(\mu\text{-}O)(\mu\text{-}OAc)_2(HBpz_3)_2]$ and $[Fe_2(\mu\text{-}O)(\mu\text{-}OAc)_2(Me_3TACN)_2]^{2+}$. The former is prepared from iron(III) perchlorate and sodium acetate, and it has characteristic UV−vis bands of the (μ-oxo)diiron(III) motif.[90,91] Together with magnetic measurements, these properties support the notion that the bridged structure remains intact in solution. Other physical measurements including Mössbauer spectroscopy (Table 3) defined the standard for (μ-oxo)bis(μ-carboxylato)diiron(III) complexes. Analogous diiron(III) compounds of similar structure and physical properties are the cationic species $[Fe_2(\mu\text{-}O)(\mu\text{-}OAc)_2(Me_3TACN)_2]^{2+}$, having one Me_3TACN ligand on each iron atom,[40] and $[Fe_2(\mu\text{-}O)(\mu\text{-}OAc)_2(TMIP)_2]^{2+}$.[92] ($\mu$-Hydroxo)bis($\mu$-carboxylato) diiron(III) analogues have also been synthesized and characterized.

Subsequently, a series of (μ-oxo)(μ-carboxylato)-diiron(III) complexes were prepared employing a variety of dinucleating ligands, including PMPE,[93] XDK,[94] and PMAPB (Figure 2),[95] or mononucleating ligands, such as PMMP,[93] EDTA derivatives,[96,97] and BPMB (Figure 2).[95] Other diiron(III) compounds reported incorporate different types of bridges, such as hydroxo, phenoxo, or alkoxo groups.[98−100]

Diiron(III) complexes of the TPA ligand and its derivatives, having (μ-oxo)(μ-hydroxo)- or di(μ-oxo)diiron(III) cores, have also been synthesized and extensively characterized.[101−103] The Fe···Fe distances in these complexes, 2.7−3.0 Å, are relatively short (Table 2), affording Fe−μ-O−Fe angles of 100° or smaller, distinctive UV−vis absorption bands (Table 5), and characteristic $\nu_{Fe-O-Fe}$ vibrations (Table 4) and spin exchange coupling constants (J values). The properties of the di(μ-oxo) derivatives are significantly different from those of mono(μ-oxo) complexes; for example, the UV−vis bands at 470 and 760 nm are shifted from ca. 550 and 800 nm (Table 5). These spectroscopic features may assist in identifying such a core structure in a metalloenzyme active site.

Scheme 6

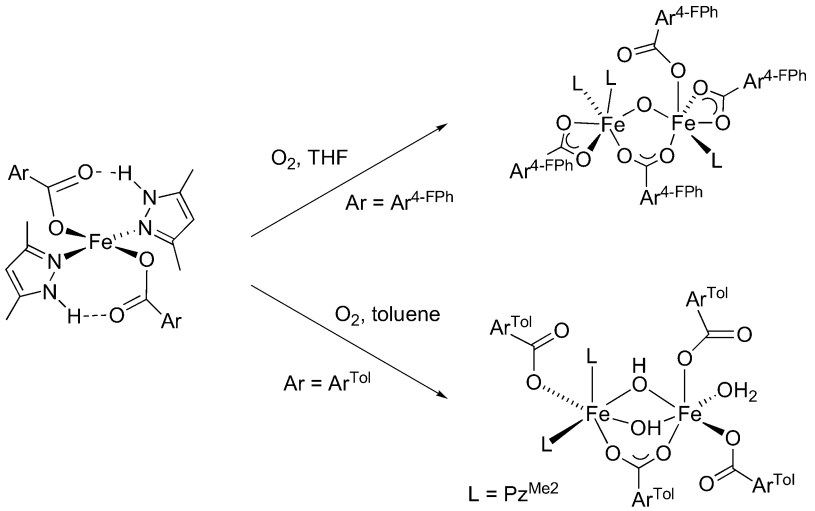

4.2. Diiron(III) Compounds Prepared from Preformed Mononuclear Complexes

A different approach to the synthesis of dinuclear iron(III) complexes is to prepare a mononuclear iron compound already complexed with one or more of the desired ligands for conversion into the desired dinuclear species upon addition of a suitable reagent. For example, the iron(III) compound $[Fe(MeIm)_6]^{3+}$ converts to a (μ-oxo)diiron(III) complex upon reaction with water in MeIm. The resulting $[Fe_2(\mu\text{-}O)(MeIm)_{10}]^{4+}$ cation, when exposed to CO_2 or following addition of a carboxylate ligand, afforded the methyl carbonate $[Fe_2(\mu\text{-}O)(\mu\text{-}O_2COCH_3)(MeIm)_6]^{3+}$ or the (μ-oxo)mono(μ-carboxylato)diiron(III) $[Fe_2(\mu\text{-}O)(\mu\text{-}O_2CR)(MeIm)_6]^{3+}$ (R = H, Me, Ph) species, respectively.[104] Attempts to add a second carboxylate unit, however, resulted in the formation of polyiron clusters. Nevertheless, this approach allowed the synthesis and evaluation of sterically unstrained (μ-carboxylato)diiron compounds that were difficult to obtain by other routes because of the formation of compounds having high nuclearity.

Another way to obtain dinuclearity is to begin with a mononuclear iron(II) compound and allow it to react with an oxidant to obtain a diiron(III) complex. For example, the cation $[Fe(6\text{-}Ph\text{-}TPA)(MeCN)_2]^{2+}$ reacts with ^{t}BuOOH to produce an equilibrium mixture of mono- and dinuclear $[Fe_2(\mu\text{-}O)((6\text{-}O\text{-}C_6H_4)TPA)_2]^{2+}$ compounds. The reaction proceeds via the formation of a mononuclear alkylperoxo intermediate.[105,106] As indicated from the formula of the final product, the pendant phenyl groups of the 6-Ph-TPA ligand become oxygenated at the *ortho* position, a feature revealed by X-ray crystallography.

Recently we developed a synthetic method to prepare diiron(III) compounds by the reaction of mononuclear iron(II) complexes with molecular oxygen.[107] The complex $[Fe_2(\mu\text{-}O)(\mu\text{-}O_2CAr^{4\text{-}FPh})(O_2CAr^{4\text{-}FPh})_3(Pz^{Me2})_3]$, which contains a ($\mu$-oxo)($\mu$-carboxylato)diiron(III) core, was obtained when the mononuclear precursor $[Fe(O_2CAr^{4-FPh})_2(Pz^{Me2})_2]$ was treated with dioxygen in THF (Scheme 6). Reaction of the closely related analogue $[Fe(O_2CAr^{Tol})_2(Pz^{Me2})_2]$ with dioxygen in toluene afforded a di(μ-hydroxo)(μ-carboxylato)diiron(III) complex, $[Fe_2(\mu\text{-}OH)_2(\mu\text{-}O_2CAr^{Tol})(O_2CAr^{Tol})_3(Pz^{Me2})_2)(OH_2)]$. These results demonstrate how the diiron(III) structures in different metalloproteins, namely, the μ-oxo cores of Hr (Scheme 1) and RNR (Scheme 2), and the di(μ-hydroxo) unit of MMOH (Figure 1), can be accessed by subtle modifications in ligand composition.

4.3. Complexes Containing Dendritic Units

In order to imitate the hydrophobic environment of the metalloprotein core, diiron complexes were synthesized with ligands containing dendritic appendages.[108] Mononuclear iron(II) poly(benzyl ether) dendrimers with TACN as the metal-binding unit were prepared from iron(II) chloride in the presence of sodium acetate. Complexes of the type $[Fe(\eta^2\text{-}OAc)(L_{n3}TACN)]^+$, where n is the generation number of the dendrimeric unit, were obtained (Scheme 7). Oxidation with O_2 gave dinuclear iron(III) complexes featuring a (μ-oxo)bis(μ-acetato) core, similar to the Me_3TACN-based nondendritic complexes discussed previously.[41] Irradiation of the diiron(III) complexes in the presence of sodium acetate gave dinuclear iron(II) compounds, which could be reoxidized by O_2 to the diiron(III) state. The diiron centers of the largest compounds, generation $n = 4$, are totally encapsulated by the large dendrimer framework. The resulting diiron(III) unit is highly robust toward alkaline hydrolysis, demonstrating the importance of the hydrophobic environment surrounding the diiron site in maintaining stability.

5. Formation of Oxygenated Intermediates

In this section we describe the activation of dioxygen by diiron(II) compounds that lead to the formation of interesting intermediates. Related species generated from reactions of diiron(III) complexes with other oxidants, such as hydrogen peroxide, are also presented. Mixed-valent diiron(II,III) compounds, which can be obtained either by direct reaction of O_2 with diiron(II) complexes, or from monomeric precursors by other methods, although not strictly "oxygenated intermediates", are also included in this section. Tables 2−5 summarize selected Fe···Fe distances,

Scheme 7

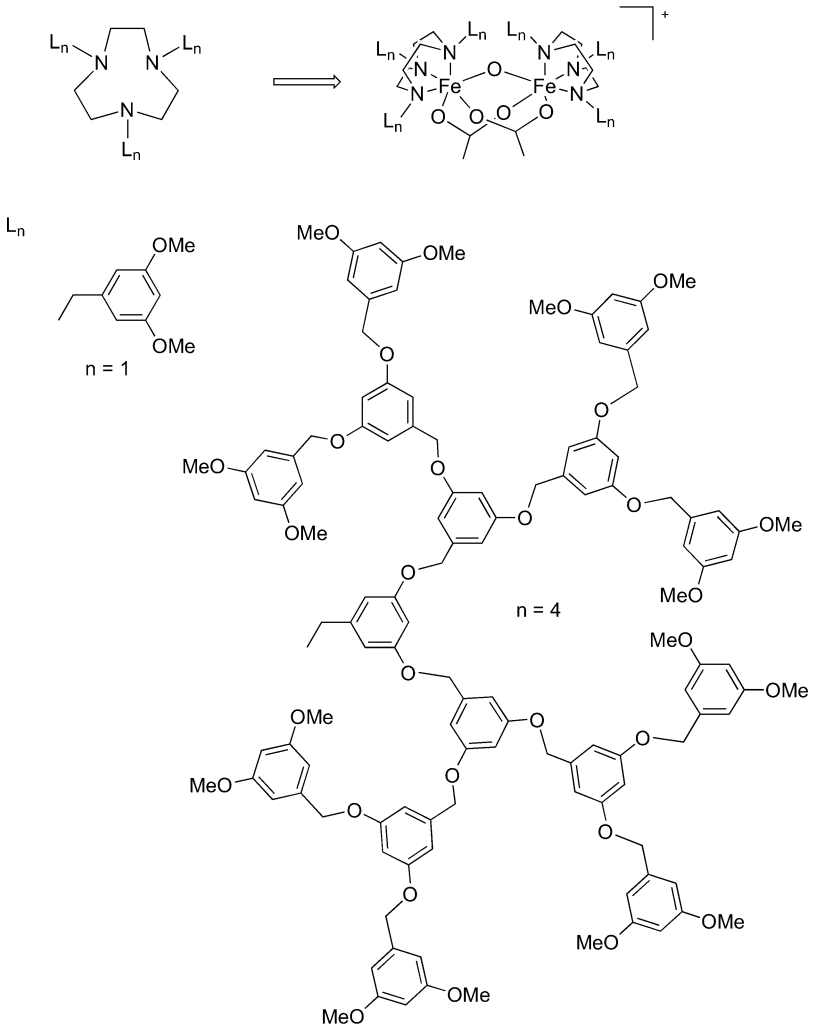

Mössbauer parameters, resonance Raman data, and electronic absorption band maxima, respectively.

5.1. Mixed-Valent Fe(II)Fe(III) Complexes

Mixed-valent Fe_2(II,III) species can be accessed for several carboxylate-bridged diiron proteins. Although not usually physiologically relevant, these mixed-valent forms have useful spectroscopic features that help to identify the diiron motif. An example is the EPR spectrum of mixed-valent MMOH,[109−111] the characteristic properties of which facilitated the assignment of its non-heme diiron centers. These units are normally antiferromagnetically coupled, resulting in an $S = {}^1/_2$ ground state. Several mixed-valent Fe_2(II,III) compounds have been synthesized as models for this form of the metalloprotein cores.

One such compound, prepared directly from an iron(III) salt, is the crystallographically characterized $[Fe_2(\mu\text{-BPMP})(\mu\text{-OPr})_2]^{2+}$ cation featuring electronic absorption maxima at 385, 554, and 1340 nm.[48,49] The Mössbauer spectrum is consistent with mixed-valent character (Table 3).

Two mixed-valent diiron(II)/(III) derivatives of the tetraaminodiphenol macrocyclic ligands L^1 and L^2 (Figure 2) were synthesized by reaction of an iron(III) precursor with an iron(II) compound.[112] The complex $[L^1Fe_2(\mu\text{-OAc})_2]^+$ (L^1 = N_4-diphenol macrocycle) displayed a single quadrupole doublet in its Mössbauer spectrum (Table 3), establishing valence-delocalized character. The complex $[L^2Fe_2(\mu\text{-OAc})(OAc)(H_2O)]^+$ (L^2 = $(NH)_4$-diphenol macrocycle), however, features two distinct doublets reflecting two discrete iron sites (Table 3), revealing valence localization and an $S = {}^9/_2$ ground spin state.

Other Fe_2(II,III) complexes were obtained upon reaction of a diiron(II) precursor with dioxygen. For example, the hydroxo-bridged $[Fe_2(\mu\text{-OH})(\mu\text{-Piv})_2(Me_3\text{-TACN})_2]^{2+}$ and μ-oxo $[Fe_2(\mu\text{-O})(\mu\text{-O}_2CCPh_3)_2(Me_3\text{-TACN})_2]^+$ cations having additional bridging carboxylate ligands were prepared by reacting the diiron(II) analogues with dioxygen.[42,113,114] These complexes were characterized crystallographically, as well as by other physical measurements including magnetic susceptibility, EPR, Mössbauer (Table 3), and resonance Raman (Table 4) spectroscopy. The results indicate that these high-spin complexes have an $S = {}^1/_2$ ground state and that outer-sphere oxidation probably occurred during their synthesis, since the bridging oxygen atom in the (μ-hydroxo)diiron(II) precursor is not exchanged with the oxidant. The ν_{as}(Fe−O−Fe) bending mode of the μ-oxo compounds is characterized by a band at 700−850 cm^{-1} in the resonance Raman spectrum (Table 4), which may serve as a useful tool for the identification of related

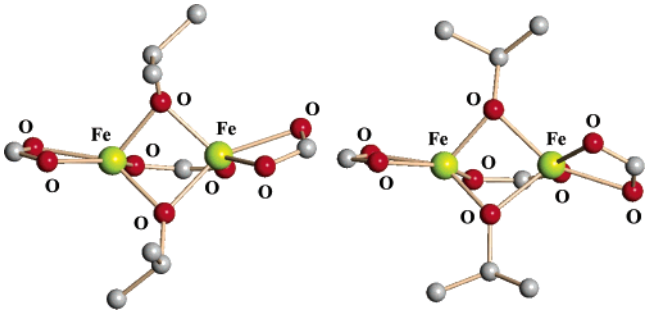

Figure 13. Two structural conformations of $[Fe_2(\mu\text{-}O_2CAr^{Mes})(\mu\text{-}O^iPr)_2(O_2CAr^{Mes})_2]$, as revealed by X-ray crystallography; all atoms of the carboxylate ligands, except for the oxygen and α-carbon atoms, are omitted for clarity.[71]

structural motifs in synthetic model systems. Since the mixed-valent species were more easily trapped upon increasing the steric bulk of the carboxylate ligands, it was proposed that steric crowding prevents carboxylate shifts,[34] processes that lead ultimately to the formation of diiron(III) complexes.[42]

Formation of mixed-valent diiron(II/III) complexes also occurs with systems supported by bulky bridging *m*-terphenyl carboxylate ligands.[62] One-electron oxidation of diiron(II) compounds of the type $[Fe_2(O_2CAr^{Tol})_4L_2]$, L = Py, ^{t}Bu-Py, or THF, was readily apparent in CV traces.[67] The resulting high-spin Fe_2(II,III) iron centers are valence-delocalized, with $S = {}^9/_2$ ground states characterized by a $g = 10$ signal in the EPR spectrum at 11 K. Direct metal−metal interactions are proposed to play an important role in facilitating spin delocalization by double exchange. These compounds display optical absorption maxima at 650−670 nm with ϵ = 1600−1700 M^{-1} cm^{-1}, features that are quite similar to those arising from the LMCT bands of peroxide−iron(III) units in peroxo-type intermediates (Table 5, vide infra). In this case, however, the green color results from an intervalence charge-transfer (IVCT) band of the diiron(II,III) unit, serving as a reminder that assignment of peroxo intermediates should not be made solely on the basis of electronic absorption spectra.

Another complex having an $S = {}^9/_2$ ground state was obtained from the reaction of the coordinatively unsaturated diiron(II) complex $[Fe_2(O_2CAr^{Mes})_2L_4]$, which has a bulkier carboxylate ligand, with dioxygen at −30 °C in 2-propanol as the solvent.[71] An X-ray crystallographic analysis of the product revealed two different structures, one completely valence-delocalized and the other having a valence-trapped state (Figure 13). One of the conformations can be represented by the formula $[Fe_2(\mu\text{-}O_2CAr^{Mes})(\mu\text{-}O^iPr)_2(O_2CAr^{Mes})_2]$, with an Fe···Fe distance of 2.62 Å (Table 2). Its metal−ligand bond lengths at 173 K indicated valence delocalization. Different crystallization conditions afforded a compound having a similar formula, but a different conformation of the bridging isopropoxide groups and an Fe···Fe distance of 2.75 Å (Table 2). An analysis of the metal−ligand bond distances suggested valence localization. These mixed-valent compounds were also characterized by UV−vis (λ_{max} = 780), Mössbauer (Table 3), EPR, and magnetic susceptibility measurements.

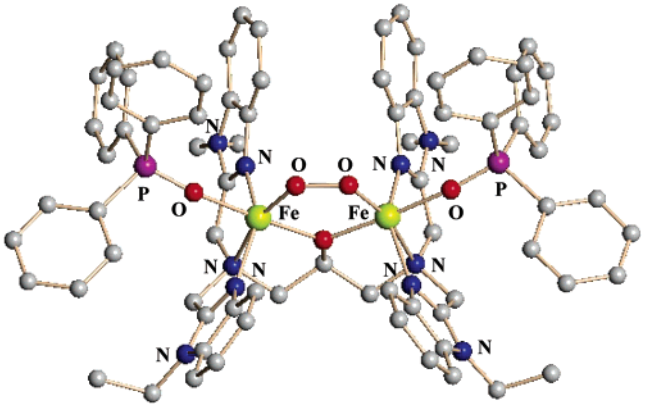

Figure 14. Structure of the peroxo-bridged complex $[Fe_2(\mu\text{-}1,2\text{-}O_2)(\mu\text{-}N\text{-Et-HPTB})(Ph_3PO)_2]^{3+}$.[118]

5.2. Diiron(III) Peroxo Complexes: Peroxo Intermediate Analogues

The first well-characterized species observed in the catalytic cycle of MMOH and related carboxylate-bridged diiron metalloenzymes, formed upon reaction of the diiron(II) state with dioxygen, is a peroxo diiron(III) intermediate (Scheme 3).[2] It is therefore of great interest to obtain synthetic complexes that mimic this dioxygen reactivity, affording (peroxo)-diiron(III) units, the characteristics of which can be compared to those formed at the enzyme active sites. In this manner, one might both contribute to our understanding of the biological systems and eventually mimic their reaction chemistry. Several diiron(III) peroxo complexes have been prepared, as described in this section.

The dinucleating ligand HPTB (Figure 2) supports diiron(II) compounds having a (μ-alkoxo)(μ-carboxylato) structure. Although not strictly reproducing the protein diiron cores, the reactivity of these complexes is of some interest. Introduction of O_2 into a methylene chloride solution of $[Fe_2(\mu\text{-}N\text{-Et-HPTB})(\mu\text{-}O_2CPh)]^{2+}$ or its HPTB-unsubstituted analogue at −80 °C resulted in species exhibiting a visible absorption band at ∼600 nm (Table 5) and resonance Raman features at 800−900 cm^{-1}, characteristic of μ-peroxo species. This unit is stabilized by polar aprotic solvents.[115−117] The use of various substituted carboxylates indicated that these ligands remain bound to the diiron center in the peroxo adducts. Crystals were grown from a solution of the dioxygen reaction product in the presence of Ph_3PO, and the resulting X-ray structure revealed an Fe−O−O−Fe moiety, in which the peroxo ligand coordinates in a *cis* μ-1,2 fashion (Figure 14). The resulting Fe···Fe separation is 3.46 Å (Table 2).[118] The benzoate group, however, was not observed in the structure, but was replaced by two molecules of Ph_3PO, one bound to each iron atom, leading to the complex $[Fe_2(\mu\text{-}1,2\text{-}O_2)(\mu\text{-}N\text{-Et-HPTB})(Ph_3PO)_2]^{3+}$. Homolytic cleavage of the O−O bond, with concomitant formation of a high-valent di(oxo) species, was proposed as a decomposition mechanism for the reactive intermediate.

Kinetic studies of the formation of peroxo-type complexes involving dinucleating, single-atom bridged ligands of this class revealed that steric factors can affect dioxygen binding and thus the reaction

Scheme 8

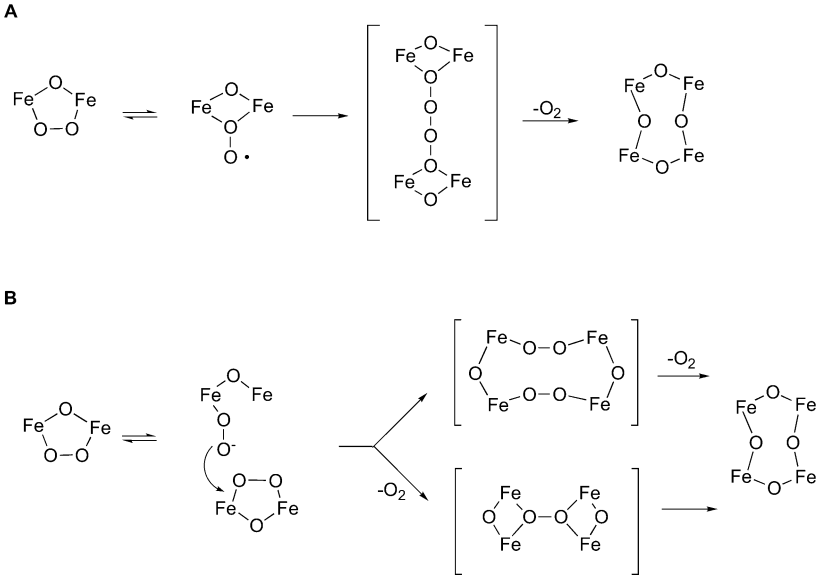

rate.[119,120] When access to the diiron center is unhindered, the reaction is first order in both dioxygen and [Fe_2(II)]. Sterically crowded compounds lowered the order with respect to dioxygen. In the latter case, a two-step mechanism was proposed, involving either ligand dissociation, or more likely, formation of a different dioxygen adduct, such as a terminal superoxide (Scheme 8). The peroxo intermediates decompose by a nonbiomimetic second-order rate-determining step, involving a bimolecular event, implying the formation of a tetranuclear species in the transition state.

Further investigation of complexes in this family of dinucleating ligands revealed that ligand steric and electronic effects strongly influence the formation and stability of the peroxo species.[50−53,121] The thermal stability of the complexes toward irreversible oxidation depends on the steric bulk of the dinucleating ligand and its electron donating ability. Electron donors facilitate formation of Fe(IV) species but inhibit return of the diiron(III) peroxo species to the diiron(II) state. In addition, introduction of methyl or phenyl substituents blocks irreversible oxidation, possibly by precluding a bimolecular decomposition pathway. Thus, weaker electron donors and sterically bulkier ligands that form a hydrophobic pocket at the O_2 binding site should stabilize the μ-peroxo species.

The crystal structure of the peroxo compound [Fe_2-(μ-1,2-O_2)(μ-Ph-BIMP)(O_2CPh)]$^{2+}$, which was obtained in a reversible reaction of the corresponding diiron(II) complex with dioxygen at ambient temperature, suggests that the phenyl groups of the Ph-BIMP ligand induce both of these desired properties (Figure 15).[122] The 4-phenyl substituents on the imidazole rings cause an elongation of the Fe−N(imidazole) bonds, which weakens the electron donor properties of the imidazole groups. The phenyl rings, not shown in the figure, also form a hydrophobic pocket surrounding the coordinated peroxide ion. The dioxygen affinity depends on the stereochemistry of the bridging skeleton. Higher affinity was observed for ligands containing the 2,6-bis(aminomethyl)phenolate moiety, compared to those of the 1,3-diamino-

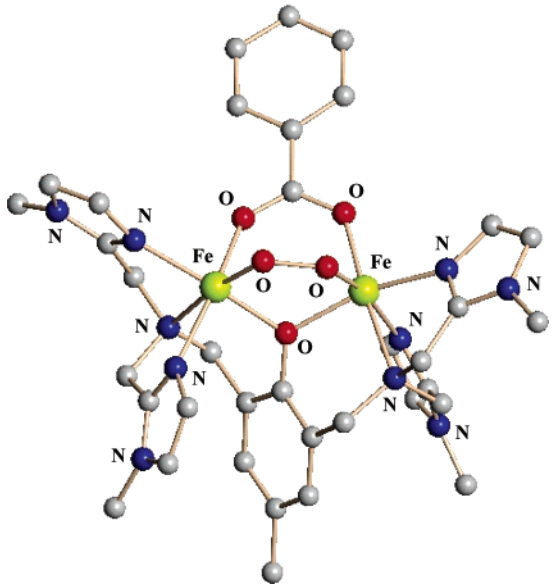

Figure 15. Structure of the peroxo-bridged complex [Fe_2-(μ-1,2-O_2)(μ-Ph-BIMP)(O_2CPh)]$^{2+}$; phenyl substituents are omitted for clarity.[122]

2-propanoate type. Peroxo complexes were also obtained in reactions of H_2O_2 with diiron(III) precursors coordinated to dinucleating ligands of this class.[98] Kinetic studies indicated that the solvent strongly affects the reaction rate and that peroxo species persist in coordinating solvents. In addition, diiron(III) peroxo complexes derived in this manner from the reaction of diiron(III) with H_2O_2 were more stable than those obtained from the reaction of the analogous diiron(II) complex with O_2.

Another ligand system that supports the formation of peroxo diiron(III) species is that based on the hydrotris(pyrazolyl)borate framework. Mononuclear iron(II) carboxylate compounds of the terminally capping ligand HB(3,5-^{i}Pr$_2$pz)$_3$, and its analogues, convert upon exposure to dioxygen to dinuclear peroxo intermediates, which are relatively stable below −20 °C. At higher temperatures they decompose ultimately to form trinuclear iron(III) com-

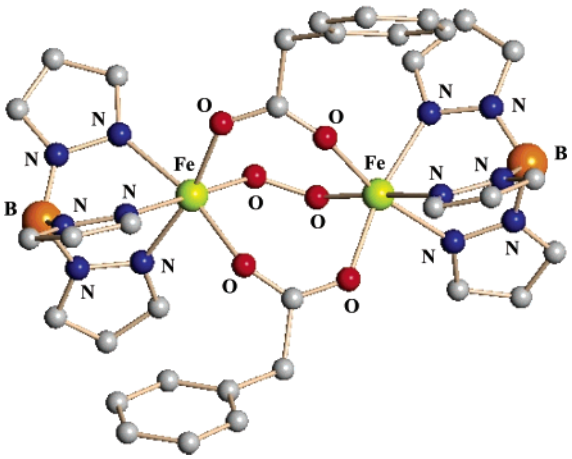

Figure 16. Structure of the peroxo-bridged complex [Fe_2(μ-1,2-O_2)(μ-O_2CCH_2Ph)$_2${HB(3,5-^{i}Pr$_2$pz)$_3$}$_2$]; ^{i}Pr substituents are omitted for clarity.[124]

plexes.[123] The assignment of the nature of the intermediates was based upon dioxygen uptake experiments, which revealed a 2:1 Fe/O_2 stoichiometry, UV−vis absorption spectral maxima around 690 nm (Table 5), resonance Raman spectroscopic data revealing ν_{O-O} at 876 cm^{-1}, and EXAFS results (Fe···Fe separation of 4.3 Å). Subsequently, a peroxo complex of this family, [Fe_2(μ-1,2-O_2)(μ-O_2CCH_2Ph)$_2$-{HB(3,5-^{i}Pr$_2$pz)$_3$}$_2$], was crystallized at −80 °C, and its structure was determined (Figure 16).[124] The peroxo unit bridges the two iron atoms in a μ-1,2 mode, which, together with the two bridging carboxylate ligands, led to an Fe···Fe separation of 4.0 Å (Table 2). In the absence of a single atom bridge, the Fe−O−O−Fe dihedral angle is 52.9°, and not 0° as observed for the previous examples.[118,122]

This compound was also examined spectroscopically. It displays a resonance Raman band corresponding to the ν_{O-O} stretching vibration at 888 cm^{-1}, which shifted to 842 cm^{-1} upon use of $^{18}O_2$ (Table 4). Its Mössbauer spectral parameters in frozen toluene solution at 4.2 K consist of a symmetric quadrupole doublet (Table 3). The similarities of these parameters to those obtained for the H_{peroxo} intermediate of MMOH (δ = 0.66 mm s^{-1}, ΔE_Q = 1.51 mm s^{-1})[13] are striking and support the assignment of the latter as a (1,2-μ-peroxo)diiron(III) intermediate. A subsequent spectroscopic study performed on the synthetic peroxo complex revealed that π-bonding between the iron atom and the peroxide unit makes a significant contribution to the interaction.[125] This study also established that the peroxide ligand has rather basic and nucleophilic character, and the authors concluded that protonation and heterolytic cleavage of the O−O bond accompany formation of high-valent di(μ-oxo)diiron(IV) species in related metalloproteins. Such a conclusion is not in accord with recent DFT calculations of H_{peroxo} to Q conversion in MMOH, however, in which O−O bond homolysis is preferred.[126]

Peroxo-type intermediates were also observed with systems containing the XDK ligand and its analogues.[59,61] Exposure of these diiron(II) complexes to O_2 at −77 °C in nonpolar solvents yielded deep blue solutions having λ_{max} ∼ 580 nm (Table 5). This irreversible oxidation reaction proceeds with 1:1 Fe_2/O_2 stoichiometry, and resonance Raman bands are consistent with the formation of a peroxo diiron(III) unit (Table 4). Mössbauer spectroscopy confirmed this assignment and indicated the presence of two inequivalent iron atoms (Table 3). Kinetic experiments revealed the reaction to be first order in both diiron(II) and dioxygen, implying a rate-determining bimolecular collision between the reactants. The rate of peroxo formation varies inversely with the steric demands of the carboxylate substituents, implying that a carboxylate shift is involved in the rate-determining step.[33,34] The oxygenation reaction is also affected by the basicity of the N-donor ligand.

Diiron(II) complexes of *m*-terphenyl carboxylate ligands display similarly interesting reactivity with dioxygen.[62] The diiron(II) compound [Fe_2(μ-O_2C-Ar^{Mes})$_2$(O_2CAr^{Mes})$_2$($MeCN$)$_2$] reacts with O_2 in noncoordinating solvents at −50 °C to give an EPR-silent intermediate that absorbs at 540 nm (Table 5).[72] The conditions employed were somewhat different from those leading to the formation of Fe_2(II,III) complexes.[71] The ν_{O-O} vibration at 885 cm^{-1} shifts by only 14 cm^{-1} upon the use of $^{18}O_2$ (Table 4), an unusually small value compared to other Fe_2(μ-1,2-peroxo) complexes and to theoretical expectations. This species is stable for at least 12 h at −50 °C, presumably because the steric bulk of the ligand inhibits decomposition processes.

Complexes derived from similar ligands behaved differently with dioxygen.[62] Whereas compounds of other relatively sterically crowded ligands in this class (Figure 2, $^-O_2CAr^{Tol}$) afford mixed-valent species (vide infra), the paddleweel diiron(II) complexes derived from the sterically less demanding ligand $^-O_2CDXL$ (Figure 2) lead to unusual peroxo-type compounds.[73] Compounds of general formula [Fe_2(μ-O_2CDXL)$_4$(L)$_2$] (L = Py, MeIm, or THF) react with O_2 at −80 °C yielding deep red-brown intermediates with λ_{max} at 500−550 nm (Table 5). These intermediates are stable for days at this temperature. Their spectroscopic features include a resonance Raman band, arising from the ν_{O-O} stretch, at 822 cm^{-1} (Table 4), which is notably lower than those of known (μ-1,2-peroxo) diiron(III) compounds, although closer to the values obtained for mononuclear non-heme iron η^2-O_2 peroxo compounds.[127] This band shifts by 43 cm^{-1} upon the use of $^{18}O_2$. The Mössbauer spectrum displays two doublets of equal intensity (Table 3), which may reflect either a mixture of two compounds or, more likely, an asymmetric complex. On the basis of these data, combined with those obtained from magnetic measurements, the intermediates were postulated either to adopt an unusual asymmetrical [Fe(η^2-O_2)(L)(μ-O_2DXL)$_4$Fe(L)] structure, or to be represented by the formula [Fe(O_2DXL)(L)(μ-1,2-O_2)(μ-O_2DXL)$_3$Fe(L)] (Figure 17).

The reactivity of the diiron(II) complex [Fe_2(μ-OH)$_2$-(6-Me_3-TPA)$_2$]$^{2+}$ with dioxygen was also investigated.[128,140] A peroxo-type intermediate was obtained upon exposure of the complex to O_2 at low temperatures (−80 to −40 °C). The reaction is first order in both diiron(II) and O_2 and uninfluenced by the addition of water. An associative mechanism was

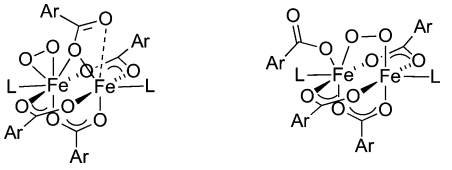

Figure 17. Two proposed peroxo structures, $[Fe_2(\eta^2\text{-}O_2)(L)(\mu\text{-}O_2DXL)_4Fe(L)]$ (left) and $[Fe_2(O_2DXL)(L)(\mu\text{-}1,2\text{-}O_2)(\mu\text{-}O_2DXL)_3Fe(L)]$ (right), for the product of the reaction $[Fe_2(\mu\text{-}O_2DXL)_4(L)_2]$ (L = Py, MeIm or THF) with O_2 at −80 °C.[73]

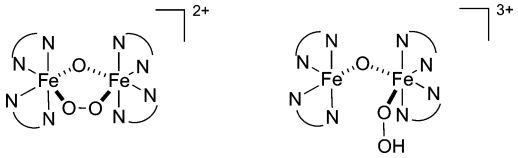

Figure 18. Two proposed structures for the products of the reaction of $[Fe_2(\mu\text{-}O)(PB)_4(H_2O)_2]^{4+}$ with H_2O_2 at −40 °C.[130,131]

proposed for the rate-determining step of the oxygenation process, on the basis of the kinetic data collected. An $\eta^1\text{-}O_2^-$ superoxo Fe_2(II,III) species was assigned as an intermediate in the reaction.

An example of a peroxo complex obtained upon activation of a diiron(III) compound with H_2O_2 is the (μ-oxo)(μ-peroxo) species $[Fe_2(\mu\text{-}O_2)(\mu\text{-}O)(\mu\text{-}OAc)(PPE)]^+$ (Figure 2), which was characterized by UV−vis spectroscopy (Table 5), elemental analysis of the OTF^- salt, FAB-MS, resonance Raman spectroscopy (816 cm^{-1} for ν_{O-O} which shifts to 771 cm^{-1} with the use of $H_2{}^{18}O_2$) (Table 4), and Mössbauer spectroscopy (one quadrupole doublet indicating a symmetric species, Table 3).[129] This peroxo species decays by a first-order process, with a relatively long half-life of 7.7 h at 300 K.

Peroxo-type compounds may be similarly obtained from the reaction of H_2O_2 with the diiron(III) complexes of the (−)4,5-pinene derivative, PB (Figure 2).[130,131] When $[Fe_2(\mu\text{-}O)(PB)_4(H_2O)_2]^{4+}$ was treated with H_2O_2 at −40 °C, a mixture of peroxo species formed. Their characterization was based on UV−vis (Table 5), EPR, Mössbauer (Table 3), and resonance Raman (867 and 806 cm^{-1}, shift to lower frequency with the use of $H_2{}^{18}O_2$) (Table 4) spectroscopic data. The products were postulated to be (μ-oxo)(μ-1,2-peroxo)diiron(III) and asymmetric (μ-oxo)-diiron(III) complexes, with the peroxo ligand in the latter binding to one of the iron atoms in a monodentate fashion (Figure 18). This species is unique in having two different local spin configurations, resulting from the binding of the hydroperoxide anion to a pyridine-rich Fe(III) center.

5.3. High-Valent Fe_2(III,IV) Complexes: Intermediate X Analogues

The R2 protein of RNR employs a formally high-valent Fe_2(III,IV) species ($S = {}^1/_2$),[32] known as "intermediate X", to generate a tyrosyl radical during catalysis.[17] This unit is formed from a peroxo diiron(III) precursor in the catalytic cycle.[2] Model compounds having such features are thus of interest to study as biomimics of this chemistry.

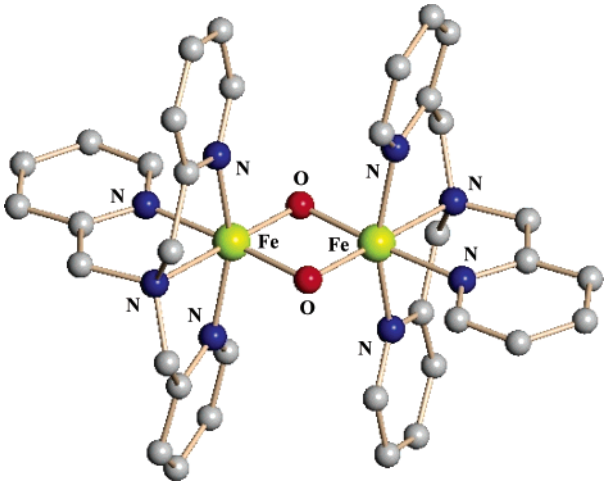

Figure 19. Structure of mixed-valent diiron(III,IV) $[Fe_2(O_2)(5\text{-}Et_3\text{-}TPA)_2]^{3+}$; ethyl substituents are omitted for clarity.[134]

A transient green species forms upon reaction of the diiron(III) complex $[Fe_2(\mu\text{-}O)(5\text{-}Me_3\text{-}TPA)_2(OH)(H_2O)]^{3+}$ with H_2O_2 at −40 °C.[115,132b] This compound exhibits electronic absorption bands at 366 and 616 nm (Table 5), an $S = {}^3/_2$ EPR spectrum with g values of 4.45, 3.90, and 2.01, Mössbauer parameters (Table 3) resulting from one sharp quadrupole doublet, and an elemental analysis corresponding to the ClO_4^- salt of the cationic complex $[Fe_2(O)_2(5\text{-}Me_3\text{-}TPA)_2]^{3+}$. From these data the compound was assigned as a valence-delocalized di(μ-oxo)Fe(III)($S = {}^1/_2$)Fe(IV)($S = 1$) complex. This conclusion was further supported by EXAFS and resonance Raman investigations. The analogous 6-Me derivative yielded a similar Fe_2(III,IV) complex, $[Fe_2(O)_2(6\text{-}Me\text{-}TPA)_2]^{3+}$. This compound is characterized by a nearly isotropic $S = {}^1/_2$ EPR signal at $g = 2.00$, however, and is an antiferromagnetically coupled system with localized high-spin Fe(III) and high-spin Fe(IV) sites.[133] In this case, the 6-methyl group appears to induce steric strain that prevents the formation of a short metal−ligand bond required for the low-spin configuration. This compound serves as a model for intermediate X in RNR. Several members of this family have been investigated. The crystal structure of the complex $[Fe_2(O)_2(5\text{-}Et_3\text{-}TPA)_2]^{3+}$ confirms the presence of the di(oxo)diiron(III,IV) unit (Figure 19).[134]

Upon reaction of the di(μ-oxo)diiron(III) complex, $[Fe_2(\mu\text{-}O)_2(6\text{-}Me_3\text{-}TPA)_2]^{3+}$,[102,115] with H_2O_2 at −40 °C, a dark green species was obtained. It has an absorption band at 648 nm (Table 5) and Mössbauer parameters (Table 3) indicative of a high-spin iron(III) sites that are antiferromagnetically coupled to afford an $S = 0$ ground state.[135] Isotope labeling MS and resonance Raman experiments (Table 4), together with EXAFS studies, assisted in assigning this compound as a symmetrical (μ-oxo)(μ-1,2-peroxo)diiron(III) species, which converts to the high-valent $[Fe_2(III,IV)(\mu\text{-}O)_2(6\text{-}Me_3\text{-}TPA)_2]^{3+}$ complex having an $S = {}^1/_2$ EPR signal at $g = 2.00$, Mössbauer parameters nearly identical to those of $[Fe_2(III,IV)(\mu\text{-}O)_2(6\text{-}Me_3\text{-}TPA)_2]^{3+}$, Table 3, and the expected mass spectrum. The system thus demonstrates that a diiron(III) peroxo-type intermediate can decompose to form high-valent Fe_2(III,IV) species, as may occur

Scheme 9

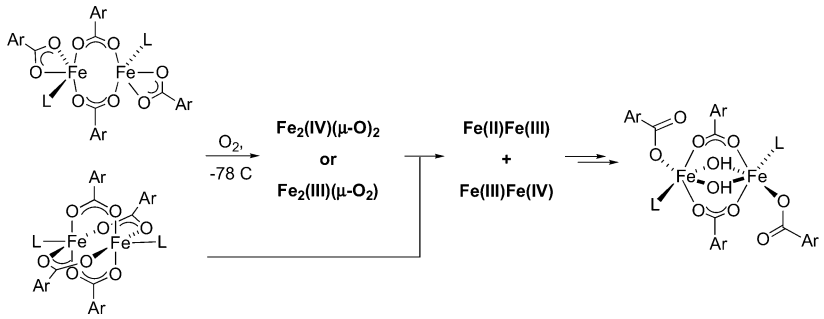

along the reaction pathway in RNR. Additional kinetic studies of the reaction of the unsubstituted analogue $[Fe_2(\mu\text{-}O)(TPA)_2(OH)(H_2O)]^{3+}$ with H_2O_2 confirmed rapid formation of the peroxo intermediate leading to the high-valent Fe_2(III,IV) compound.[136] The complex $[Fe_2(III,IV)(\mu\text{-}O)_2(6\text{-}Me_3\text{-}TPA)_2]^{3+}$ was also obtained by one-electron oxidation of the $[Fe(III)Fe(III)(\mu\text{-}O)_2(6\text{-}Me_3\text{-}TPA)_2]^{2+}$ precursor. It was further shown by resonance Raman experiments that the $Fe_2(\mu\text{-}O)_2$ core isomerizes to give an Fe(III)−O−Fe(IV)═O structure, demonstrating its flexibility.[137] Although this system appears to be the realization of a model postulated for the high-valent Fe_2(IV)-$(\mu\text{-}O)_2$ core in MMOH intermediate Q, based on computational studies that propose a similar isomerization,[138] other evidence indicates that Q is a di(μ-oxo)diiron(IV) unit, especially the Fe···Fe distance of 2.46 Å obtained from EXAFS spectroscopy.[139] Intermediate Q is directly responsible for substrate oxidation in MMOH and does not appear to require isomerization to a different structure.

Further progress toward mimicking the oxygenation pathway in metalloenzymes was achieved when the diiron(II) compound $[Fe_2(\mu\text{-}OH)_2(6\text{-}Me_3\text{-}TPA)_2]^{2+}$ was allowed to react with O_2 at −40 °C.[140] An EPR-silent peroxo species, assigned on the basis of UV−vis spectral (λ_{max} = 640 nm) (Table 5), MS, and resonance Raman studies (Table 4), initially forms and then decays, giving rise to an EPR signal at g = 1.999, which is similar to the one obtained for the Fe_2(III,IV) complex described above. In a manner resembling RNR−R2, this system converts 2,4,6-tri-*tert*-butylphenol to the phenoxyl radical. This example represents a closer mimic of the natural processes, because the precursor compound is a diiron(II) complex and dioxygen serves as the oxidant.

An inherently different system for converting a diiron(II) precursor with dioxygen to a mixed-valent diiron(III)(IV) species is one derived from the *m*-terphenyl carboxylate ligand family (Figure 2).[62,63,68] Upon reaction with dioxygen, diiron(II) complexes of the type $[Fe_2(O_2CAr^{Tol})_4(L)_2]$, where L = Py or ^{t}Bu-Py, convert ultimately to di(μ-hydroxo)diiron(III) compounds. Dark green intermediates in this pathway were characterized by low-temperature UV−vis ($\lambda_{max} \sim 660$ nm), EPR ($g = 2$, $g = 10$), and Mössbauer spectroscopic studies. The spectra revealed the products to contain a 1:1 mixture of valence-delocalized Fe_2(II,III) and valence-trapped Fe_2(III,IV) species, the rates of formation of which are identical. The proposed chemical transformations are illustrated in Scheme 9. This system can also convert 2,4,6-tri-*tert*-butylphenol to the phenoxyl radical, and 2,4-di-*tert*-butylphenol to the corresponding biphenol. The chemistry is of significance as a structural and functional model of the active site of the metalloenzymes in their reduced states. The ligand composition matches that of the enzymes, and the oxidation pathway, beginning with the reaction of a diiron(II) precursor and dioxygen and possibly traversing the diiron(IV) state, parallels that found in nature.

5.4. High-Valent Fe_2(IV) Complexes: Intermediate Q Analogues

The reactive species responsible for methane oxidation in MMOH is assigned as a high-valent di(μ-oxo)diiron(IV) unit.[13,32] The synthesis of analogous small molecule model compounds has been a challenge. Recently, a diiron compound having such a diiron(IV) core has been prepared in a nonbiomimetic fashion from the mononuclear precursor [Fe(BPMCN)$(OTf)_2$] and the oxidant ^{t}BuOOH at −80 °C. The reaction appears to proceed via the peroxo species Fe(III)−O−O− ^{t}Bu.[141] This "Q-type" compound exhibits UV−vis absorption maxima (−80 °C) at λ_{max} of 656 and 845 nm (Table 5), and a solid sample was characterized by elemental analysis. Its Mössbauer spectrum displays a single sharp quadrupole doublet (Table 3), comparable to that of other $S = 1$ Fe(IV) sites,[142,143] but unlike that of the $S = 0$ intermediate Q.[13] The resonance Raman spectrum includes bands at 686, 679, and 653 cm^{-1}, which downshift to 658 and 627 cm^{-1} when ^{t}Bu^{16}O^{18}OH is used (Table 4). These observed shifts are in good agreement with the values calculated from Hooke's law for Fe−O vibrations, thus indicating incorporation of the terminal oxygen atom in the oxidant. An Fe═O site is ruled out by the lack of a band in the 800−850 cm^{-1} range.[137] EXAFS studies also support the existence of a di(μ-oxo)diiron(IV) core, with an Fe···Fe distance of 2.81 Å (Table 2). This high-valent species is reactive in the oxidation of hydrocarbons (vide infra). The compound, $[Fe_2(\mu\text{-}O)_2(BPMCN)_2]^{4+}$, although different from intermediate Q in MMOH with respect to its ligand environment, electronic spin, and mode of generation, is nonetheless the only synthetic analogue of this intermediate reported thus far that reproduces the oxidation states, bridging units, and in part the hydrocarbon oxidation reactivity of the enzyme.

6. Functional Models

The inspiration for synthetic model chemistry of non-heme diiron metalloprotein cores is first and foremost to mimic biological function. The purpose of much basic research, including attempts to determine the structures and oxidation mechanisms of the synthetic inorganic compounds described herein, is to progress in a stepwise manner toward this ultimate goal. Special interest thus derives from developing synthetic systems that not only model the diiron proteins structurally, but which also can serve as functional mimics, exhibiting substrate oxidation activity. One must distinguish between processes that proceed via dioxygen activation at the dimetallic center in a biomimetic fashion, and radical reactions that exclude actual participation of the metal active site. The latter transpire especially when oxidants such as hydrogen peroxide or alkyl hydroperoxides are employed.[9,35] Since detailed descriptions of such processes, including Gif chemistry[144−146] and Fenton type radical reactions,[147−150] are available elsewhere, only selected systems that participate in substrate oxidation, presumably in a metal-based fashion, are described in the present section. Systems operating in a stoichiometric manner with possible irreversible decomposition of the metal complex will be addressed, as will those enabling full catalytic redox cycles.

6.1. Stoichiometric Substrate Oxidation by Defined Reactive Intermediates

The syntheses of several reactive intermediates, made possible by the chemistry discussed in the previous section, enabled an evaluation of their oxidative reactivity. Consider, for example, diiron(II) complexes of dinucleating ligands that produce (1,2-μ-peroxo)diiron(III) intermediates upon reaction with dioxygen.[116] When the peroxo adduct of one such complex, $[Fe_2(\mu\text{-TPDP})(\mu\text{-}O_2CPh)]^{2+}$, was allowed to react with 2,4-di-*tert*-butylphenol, the decomposition of the intermediate was accelerated and a 50% yield of the diphenol was obtained. Similarly, reaction with Ph_3P yielded 60% of the Ph_3PO. No reaction was observed with styrene or cyclohexane.

High-valent diiron(III)/(IV) complexes are also active oxidants.[63,140,151] The TPA-based system $[Fe_2(\mu\text{-}O)_2(TPA)_2]^{3+}$ quantitatively oxidizes 2,4-di-*tert*-butylphenol to the corresponding biphenol in a $1e^-$ oxidation process, with concomitant reduction of the iron compound to the (μ-oxo)diiron(III) state.[151] This process resembles the oxidation reaction catalyzed by RNR−R2, where the mixed-valent intermediate X transforms to the (μ-oxo)diiron(III) resting state as the active site tyrosine is oxidized to the tyrosyl radical.[15] In addition, hydrocarbons are oxidized by similar $1e^-$ steps; cumene is converted ultimately to cumyl-alcohol and 1-methylstyrene, and ethyl benzene to 1-phenyl ethanol and styrene. The hydroxylation reactions mimic those obtained with sMMO,[13] and the desaturation reactions those of Δ9D.[4] Cycloheptane, however, was not oxidized. Kinetic studies suggested that cleavage of the α-C−H bond is a significant component of the rate-determining step of the reaction with hydrocarbons, with the desaturation reaction involving asynchronous scission of the two C−H bonds, as was reported for Δ9D.[152]

The Fe_2(III,IV) complexes derived from the bulky carboxylate $^-O_2CAr^{Tol}$ ligand also display oxidative reactivity.[63] The equimolar mixture of Fe_2(II,III) and Fe_2(III,IV) compounds oxidizes 2,4-di-*tert*-butylphenol to the diphenol in 40% yield relative to the starting diiron(II) center, which amounts to quantitative conversion based on the amount of Fe(IV) in solution. The reactive species, a high-valent Fe_2(III,IV) complex, thus mimics the chemistry of RNR−R2.[15]

The diiron(IV) compound $[Fe_2(\mu\text{-}O)_2(BPMCN)_2]^{4+}$, the core of which is a structural mimic of intermediate Q,[13] has stronger oxidizing power.[141] This complex can serve as a $2e^-$ oxidant, reacting with unactivated aliphatic C−H bonds, such as that in adamantane, yielding 56% of 1-adamantanol and 20% of 2-adamantanone.

6.2. "In Situ" Oxidation by Diiron(III) Precursors with H_2O_2 as the Oxidant

The (μ-oxo)(μ-acetato)diiron(III) derivative of the ligand MBEN (Figure 2) reacts with H_2O_2 or O_2 in the presence of excess ascorbate to give a mononuclear complex in which one of the aromatic rings of the ligand is hydroxylated.[96,97] The oxidized ligand could be isolated in 80% yield.

In related chemistry, a (μ-oxo)(μ-acetato)diiron(III) compound was obtained by allowing the mononuclear iron(II) complex $[Fe(MPED)(MeCN)_2]$ to react with acetic acid in the presence of H_2O_2.[153a] A mixture of these components was able to catalyze the epoxidation of a variety of olefins. Although detailed mechanistic aspects of this reaction have not yet been addressed, it was established that the diiron compound could promote catalysis and afford better yields than those derived from the mononuclear compound in the absence of acetic acid. The nature of the catalyst has not yet been determined, and recent work has questioned whether a dinuclear complex plays a role in the catalysis.[153b]

Another example is a catalytic oxidation induced by a diiron(III) compound in the presence of H_2O_2 that occurs in an enantioselective manner.[131,154] As previously discussed, the diiron(III) compound $[Fe_2(\mu\text{-}O)(PB)_4]^{4+}$ converts to a peroxo-type species upon reaction with H_2O_2. In the presence of the oxidant, this complex is active in catalytic enantioselective sulfoxidation of a variety of sulfides. Since the only source of optical activity is the ligand coordinated to the iron atoms, it was concluded that catalysis proceeds via a metal-based process and that the peroxo moiety is the actual oxygen atom donor to the substrate. In addition, it was established that dinuclear catalysts are more reactive and enantioselective than their mononuclear counterparts.

6.3. "In Situ" Oxidation by Diiron(II) Precursors with O_2 as the Oxidant

Since the native systems activate diiron(II) centers with dioxygen, synthetic models that mimic such a pathway are of great value. One interesting example

Scheme 10

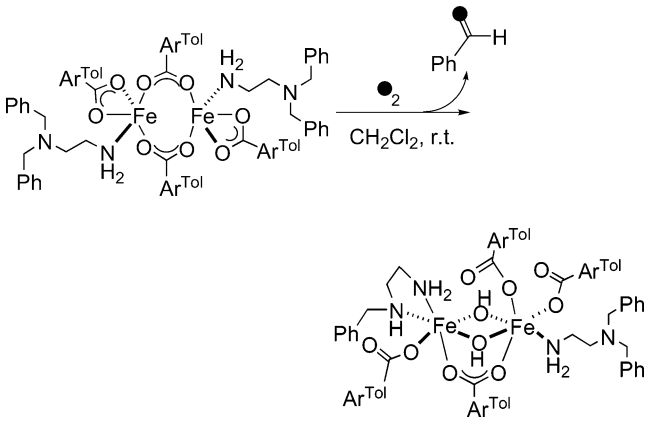

of such in situ dioxygen activation of a diiron(II) precursor that leads to substrate oxidation is that formed from the bulky $^{-}O_2CAr^{Tol}$ carboxylate ligand.[62,64,66] As discussed above, diiron(II) complexes of the type $[Fe_2(O_2CAr^{Tol})_4L_2]$, where L is a terminal N-donor ligand, convert, upon reaction with O_2 at low temperature, to mixed-valent Fe_2(III,IV) species. The pathway for this conversion has been postulated to include a di(μ-oxo)diiron(IV) intermediate (Scheme 9). When L is *N*,*N*-dibenzyl-ethylenediamine, the terminal ligand binds to the iron(II) atom in a monodentate mode via the unsubstituted, less sterically crowded nitrogen atom. Upon introduction of dioxygen, the complex converts to a di(μ-hydroxo)(μ-carboxylato)diiron(III) species (Scheme 10)[64] that precisely models the core in the resting, oxidized state of MMOH.[13] Crystallographic characterization of this diiron(III) compound reveals that one of the benzyl substituents on one of the two N-donor ligands is replaced with a hydrogen atom, leading to bidentate binding of that ligand to one Fe(III) center. Moreover, benzaldehyde forms in 60% yield. This system thus provides the first example of intramolecular oxidative N-dealkylation by reaction of a diiron(II) precursor with dioxygen, presumably via an Fe(IV)Fe(IV) intermediate. In more recent work,[155] several other ligands with appended substrate moieties were oxidized in an intramolecular fashion, including benzylamine, 4-methoxybenzylamine, and benzyl groups as well as heteroatomic units such as sulfides and phosphines attached to pyridine.

Another example of a catalytic reaction promoted by a diiron(II) precursor and dioxygen is one based on the complex $[Fe_2(\mu\text{-}O_2CAr^{Tol})_2(Me_3TACN)_2(MeCN)_2]^{2+}$.[156] This cation reacts with dioxygen and, presumably via a peroxo intermediate, generates the (μ-oxo)diiron(III) derivative. Both the diiron(II) precursor and the resulting (μ-oxo)diiron(III) compound catalytically convert Ph_3P to Ph_3PO in the presence of excess dioxygen, with the highest turnover number obtained thus far being >4000. Although experiments performed in the presence of a radical scavenger, EPR measurements, and other information suggested that the reaction does not proceed via a radical mechanism,[156] additional studies of this oxidation reaction are being undertaken and at present we do not rule out such a possibility.[157]

7. Summary and Perspective

Significant progress has been made in recent years in the field of small molecule modeling of carboxylate-bridged diiron metalloproteins. Many diiron(II) systems have been synthesized that mimic certain aspects of the structure of the protein active sites in their reduced state. Several (μ-oxo)- and (μ-hydroxo)-diiron(III) compounds are available that model the resting, oxidized states of these proteins. Of greater interest is that several high-valent intermediates have been identified, which share similarities with the activated diiron centers in the natural systems. Some of these systems oxidize substrates in a metal-based fashion. Although we have limited our discussion mainly to complexes containing carboxylate-bridged diiron units, other functionally relevant systems are providing important insights into the chemistry of such high-valent intermediates.[168]

Despite these accomplishments, several important goals of synthetic modeling chemistry remain to be achieved. The need to mimic the hydrophobic environment created in nature by the protein, by producing such an environment for the synthetic diiron center, is expected to be a challenge for some time to come. This requirement may be met by employing different sterically hindered ligands, the generation of dendritic units, or the use of 4-helix bundles. In addition, closer inspection of the biological active sites, and careful evaluation of differences between these systems and the synthetic ones, may assist in designing better models. One such example is the need to develop systems featuring two N-donor ligands in a *syn* configuration with respect to the Fe−Fe axis. Moreover, we still do not fully understand the exact mechanism of action of the diiron metalloenzymes, and when this information becomes available there will be additional challenges. Further mechanistic studies of active intermediates and oxidation reactivity are essential in order to compare the synthetic systems to the biological ones.

From these considerations it is clear that much remains to be discovered. The forthcoming years should bring new molecules designed to fulfill the ultimate goal of biomimetic diiron chemistry. Exciting times lie ahead.

8. Abbreviations

BBBAN	2,7-bis{2-[2-(1-methyl)benzimidazol-ethyl]-*N*-benzylaminomethyl}-1,8-2-naphthyridine
BDPTZ	1,4-bis(2,2′-dipyridylmethyl)phthalazine
BEAN	2,7-bis(*N*,*N*-diethylaminomethyl)-1,8-naphthyridine
BEN	*N*,*N*′-dibenzylethylenediamine *N*,*N*′-diacetic acid
BIPhMe	bis(1-methylimidazol-2-yl)phenyl-methoxymethane
BPMAN	2,7-bis[bis(2-pyridylmethyl)aminomethyl]-1,8-naphthyridine
BPMB	2-[(2,2-bipyrid-6-yl)-methoxy]benzoic acid

BPMCN	*N*,*N*′-bis(2-pyridylmethyl)-*N*,*N*′-dimethyl-*trans*-1,2-diaminocyclohexane
BQPA	bis(2-quinolylmethyl)(2-pyridylmethyl)amine
BuIm	butylimidazole
BZEN	benzylethylenediamine
BzIm	2-benzimidazole
(*p*-Cl)O_2CPh	*para*-chlorobenzoate
CV	cyclic voltammetry
Cy	cyclohexyl
DBEN	*N*,*N*-dibenzylethylendiamine
DMEN	*N*,*N*-dimethylethylenediamine
DPE	dipyrrolidinoethane
EDTA	ethylenediamine tetracarboxylic acid
EN	ethylenediamine
EPR	electron paramagnetic resonance
N-Et-HPTB	*N*,*N*,*N*′, *N*′-tetrakis(*N*″-ethyl-2-benzylimidazolylmethyl)-2-hydroxo-1,3-diaminopropane
5-Et_3-TPA	tris[(5-ethyl-2-pyridyl)methyl]amine
EXAFS	extended X-ray absorption fine structure
FAB	fast atom bambardment
HBHA	[(2-hydroxybenzyl)(2-imidazol-2-yl)ethyl]amine
HBIMEN	*N*-(hydroxyethyl)-*N*,*N*′,*N*,-tris(2-benzimidazolylmethyl)-1,2-diaminoethane
H_3BIOMP	2,6-bis[((2-hydroxybenzyl)((1-methylimidazol-2-yl)methyl)amino)methyl]-4-methylphenol
HB(3,5-$^{i}Pr_2$pz)$_3$	hydrotris(3,5-diisopropylpyrazol-1-yl)-borate
HBPMP	2,6-bis[(bis(2-pyridylmethyl)amino)-methyl]-4-methylphenol
HBpz_3	hydrotris-1-(pyrazolyl)borate
H-EtOH-HPTB	*N*,*N*,*N*′,*N*′-tetrakis(*N*″(2-hydroxyethyl)-2-benzylimidazolylmethyl)-2-hydroxo-1,3-diaminopropane
H_2HBAB	1,2-bis(2-hydroxybenzamido)benzene
HMe_2TPDO	*N*,*N*-bis(6-methyl-2-pyridylmethyl)-*N*′,*N*′-bis(2-pyridylmethyl)-2-hydroxy-1,3-diaminopropane
HMe_4TPDO	*N*,*N*,*N*′,*N*′-tetrakis(6-methyl-2-pyridylmethyl)-2-hydroxy-1,3-diaminopropane
$HO_2CAr^{4\text{-}FPh}$	2,6-bis(*p*-fluorophenyl)benzoic acid
HO_2CAr^{Mes}	2,6-bis(mesityl)benzoic acid
HO_2CAr^{tBu}	2,6-bis(*p*-*tert*-butyl-phrnyl)benzoic acid
HO_2CAr^{Tol}	2,6-bis(*p*-tolyl)benzoic acid
HPh-BIMP	2,6-bis[bis{2-(1-methyl-4,5-diphenylimidazolyl)methyl}aminomethyl]-4-methylphenol)
H_2Ph_4DBA	dibenzofuran-4,6-bis(diphenylaceticacid)
HPh-TIDP	*N*,*N*,*N*′,*N*′-tetrakis{2-(1-methyl-4,5-diphenylimidazolyl)methyl}-1,3-diaminopropan-2-ol
HPTB	*N*,*N*,*N*′,*N*′-tetrakis(2-benzylimidazolylmethyl)-2-hydroxo-1,3-diaminopropane
Hr	hemerythrin
HTPDP	*N*,*N*,*N*′,*N*′-tetrakis(2-pyridylmethyl)-2-hydroxy-1,3-diaminopropane
HTPPDO	*N*,*N*,*N*′,*N*′-tetrakis(6-pivalamido-2-pyridylmethyl)-1,3-diaminopropane-2-ol
H_2XDK	*m*-xylenediamine bis(Kemp's triacid)-imide
ImH	imidazole
Lut	lutidine
MBEN	*N*,*N*′-bis(3,4,5-trimethoxybenzyl)ethylenediamine *N*,*N*′-diacetic acid
Me_2HPTB	*N*,*N*,*N*′,*N*′-tetrakis(5,6-dimethyl-2-benzylimidazolylmethyl)-2-hydroxo-1,3-diaminopropane
MeIm	*N*-methylimidazole
6,6-Me_2-6-Ph-TPA	[(6-phenyl-2-pyridyl)methyl]-bis[(6,6-dimethyl-2-pyridyl)methyl]amine
MMO	methane monooxygenase
MMOH	methane monooxygenase hydroxylase
MMOR	methane monooxygenase reductase
MPED	*N*,*N*′-dimethyl-*N*,*N*′-bis(2-pyridylmethyl)-ethane-1,2-diamine
MS	mass spectrometry
Me_3TACN	1,4,7-trimethyl-1,4,7-triazacyclononane
6-Me-TPA	[(6-methyl-2-pyridyl)methyl]-bis(2-pyridylmethyl)amine
5-Me_3-TPA	tris[(5-methyl-2-pyridyl)methyl]-amine
6-Me_3-TPA	tris[(6-methyl-2-pyridyl)methyl]-amine
4,6-Me_6-TPA	tris[(4,6-dimethyl-2-pyridyl)methyl]-amine
PB	(−)4,5-pinene derivative of 2,2′-bipyridine
PEEN	*N*,*N*′-diethyl-*N*,*N*′-bis(2-pyridylmethyl)ethane-1,2-diamine
Ph_4BDPTZ	1,4-bis[bis(6-phenyl-2-pyridyl)methyl]-phthalazine
6-Ph-TPA	[(6-phenyl-2-pyridyl)methyl]-bis(2-pyridylmethyl)amine
Piv	pivalate
PMAPB	2,6-bis{[*N*,*N*-di(2-pyridylmethyl)amino]-propoxyl}benzoic acid
PMEN	*N*,*N*′-dimethyl-*N*,*N*′-bis(2-pyridylmethyl)ethane-1,2-diamine
PMMP	2-(bis(2-pyridyl)methyl)-6-methylpyridine
PMPE	1,2-bis[2-(bis(2-pyridyl)methyl)-6-pyridyl]ethane
PPE	1,2-bis[2-bis(2-pyridyl)-6-pyridyl]ethane
Py	pyridine
Pz^{Me2}	3,5-dimethylpyrazole
Pz^{iPr2}	3,5-diisopropylpyrazole
RNR	ribonucleotide reductase
sMMO	soluble methane monooxygenase
TACN	1,4,7-triazacyclononane
THF	tetrahydrofuran
TMEN	*N*,*N*,*N*′,*N*′-tetramethylethylenediamine
TMIP	tris(methylimidazol-2-yl)phosphine
TPA	tris(2-pyridylmethyl)amine
XDK	acid anion of H_2XDK

9. Acknowledgments

Studies from our laboratory were generously supported by grants from the National Science Foundation and the National Institute of General Medical Sciences. We thank all the researchers for the hard work that brought about the progress described here.

10. References

(1) Lee, D.; Lippard, S. J. In *Comprehensive Coordination Chemistry II; From Biology to Nanotechnology*; Elsevier Ltd.: Oxford, 2004; Vol. 8, p 309.
(2) Solomon, E. I.; Brunold, T. C.; Davis, M. I.; Kemsley, J. N.; Lee, S.-K.; Lehnert, N.; Neese, F.; Skulan, A. J.; Yang, Y.-S.; Zhou, J. *Chem. Rev.* **2000**, *100*, 235.
(3) Kurtz, D. M., Jr. *J. Biol. Inorg. Chem.* **1997**, *2*, 159.
(4) Wallar, B. J.; Lipscomb, J. D. *Chem. Rev.* **1996**, *96*, 2625.

(5) Babcock, G. T.; Floris, R.; Nilsson, T.; Pressler, M.; Varotsis, C.; Vollenbroek, E. *Inorg. Chim. Acta* **1996**, *243*, 345.
(6) Nordlund, P.; Eklund, H. *Curr. Opin. Struct. Biol.* **1995**, *5*, 758.
(7) Vincent, J. B.; Olivier-Lilley, G. L.; Averill, B. A. *Chem. Rev.* **1990**, *90*, 1447.
(8) Du Bois, J.; Mizoguchi, T. J.; Lippard, S. J. *Coord. Chem. Rev.* **2000**, *200−202*, 443.
(9) Fontecave, M.; Ménage, S.; Duboc-Toia, C. *Coord. Chem. Rev.* **1998**, *178−180*, 1555.
(10) Feig, A. L.; Lippard, S. J. *Chem. Rev.* **1994**, *94*, 759.
(11) Kurtz, D. M., Jr. *Chem. Rev.* **1990**, *90*, 585.
(12) Stenkamp, R. E. *Chem. Rev.* **1994**, *94*, 715.
(13) Merkx, M.; Kopp, D. A.; Sazinsky, M. H.; Blazyk, J. L.; Müller, J.; Lippard, S. J. *Angew. Chem., Int. Ed.* **2001**, *40*, 4000.
(14) Rosenzweig, A. C.; Frederick, C. A.; Lippard, S. J.; Nordlund, P. *Nature* **1993**, *366*, 537.
(15) Jordan, A.; Reichard, P. *Annu. Rev. Biochem.* **1998**, *67*, 71.
(16) Logan, D. T.; Su, X.-D.; Åberg, A.; Regnström, K.; Hajdu, J.; Eklund, H.; Nordlund, P. *Structure* **1996**, *4*, 1053.
(17) Stubbe, J. *Curr. Opin. Chem. Biol.* **2003**, *7*, 183.
(18) Westerheide, L.; Pascaly, M.; Krebs, B. *Curr. Opin. Chem. Biol.* **2000**, *4*, 235.
(19) Rosenzweig, A. C.; Feng, X.; Lippard, S. J. In *Applications of Enzyme Biotechnology*; Kelly, J. W., Baldwin, T. O., Eds.; Plenum Press: New York, 1991.
(20) *CRC Handbook of Chemistry and Physics*; CRC Press: Boca Raton, FL, 71st Ed., 1990−1991.
(21) (a) Ambundo, E. A.; Friesner, R. A.; Lippard, S. J. *J. Am. Chem. Soc.* **2002**, *124*, 8770. (b) Fuse, H.; Ohta, M.; Takimura, O.; Murakami, K.; Inoue, H.; Yamaoka, Y.; Oclarit, J. M.; Omori, T. *Biosci. Biotech. Biochem.* **1998**, *62*, 1925.
(22) Ruzicka, F.; Huang, D.-S.; Donnelly, M. I.; Frey, P. A. *Biochemistry* **1990**, *29*, 1696.
(23) Fox, B. G.; Borneman, J. G.; Wackett, L. P.; Lipscomb, J. D. *Biochemistry* **1990**, *29*, 6419.
(24) Green, J.; Dalton, H. *J. Biol. Chem.* **1989**, *264*, 17698.
(25) Colby, J.; Stirling, D. I.; Dalton, H. *Biochem. J.* **1977**, *165*, 395.
(26) Lippard, S. J. *Nature* **2002**, *416*, 587.
(27) Lippard, S. J.; Berg, J. M. *Principles of Bioinorganic Chemistry*; University Science Books: Mill Valley, CA, 1994.
(28) Holm, R. H.; Kennepohl, P.; Solomon, E. I. *Chem. Rev.* **1996**, *96*, 2239.
(29) Que, L., Jr. *J. Chem. Soc., Dalton Trans.* **1997**, 3933.
(30) Tolman, W. B.; Spencer, D. J. E. *Curr. Opin. Chem. Biol.* **2001**, *5*, 188.
(31) Lippard, S. J. *Angew. Chem., Int. Ed. Engl.* **1988**, *27*, 344.
(32) Que, L., Jr.; Tolman, W. B. *Angew. Chem., Int. Ed.* **2002**, *41*, 1114.
(33) Whittington, D. A.; Lippard, S. J. *J. Am. Chem. Soc.* **2001**, *123*, 827.
(34) Rardin, R. L.; Tolman, W. B.; Lippard, S. J. *New. J. Chem.* **1991**, *15*, 417.
(35) Costas, M.; Chen, K.; Que, L., Jr. *Coord. Chem. Rev.* **2000**, *200−202*, 517.
(36) Tolman, W. B.; Liu, S.; Bentsen, J. G.; Lippard, S. J. *J. Am. Chem. Soc.* **1991**, *113*, 152.
(37) Tolman, W. B.; Bino, A.; Lippard, S. J. *J. Am. Chem. Soc.* **1989**, *111*, 8522.
(38) Feig, A. L.; Masschelein, A.; Bakac, A.; Lippard, S. J. *J. Am. Chem. Soc.* **1997**, *119*, 334.
(39) Lachicotte, R.; Kitaygorodskiy, A.; Hagen, K. S. *J. Am. Chem. Soc.* **1993**, *115*, 8883.
(40) Hartman, J. R.; Rardin, R. L.; Chaudhuri, P.; Pohl, K.; Wieghardt, K.; Nuber, B.; Weiss, J.; Papaefthymiou, G. C.; Frankel, R. B.; Lippard, S. J. *J. Am. Chem. Soc.* **1987**, *109*, 7387.
(41) Chaudhuri, P.; Wieghardt, K.; Nuber, B.; Weiss, J. *Angew. Chem., Int. Ed.* **1985**, *24*, 778.
(42) Payne, S. C.; Hagen, K. S. *J. Am. Chem. Soc.* **2000**, *122*, 6399.
(43) Ménage, S.; Zang, Y.; Hendrich, M. P.; Que, L., Jr. *J. Am. Chem. Soc.* **1992**, *114*, 7786.
(44) Hazell, R.; Jensen, K. B.; McKenzie, C. J.; Toftlund, H. *J. Chem. Soc., Dalton Trans.* **1995**, 707.
(45) Reynolds, R. A., III; Dunham, W. R.; Coucouvanis, D. *Inorg. Chem.* **1998**, *37*, 1232.
(46) Coucouvanis, D.; Reynolds, R. A., III; Dunham, W. R. *J. Am. Chem. Soc.* **1995**, *117*, 7570.
(47) Hagen, K. S.; Lachicotte, R. *J. Am. Chem. Soc.* **1992**, *114*, 8741.
(48) Borovik, A. S.; Hendrich, M. P.; Holman, T. R.; Münck, E.; Papaefthymiou, V.; Que, L., Jr. *J. Am Chem. Soc.* **1990**, *112*, 6031.
(49) Borovik, A. S.; Papaefthymiou, V.; Taylor, L. F.; Anderson, O. P.; Que, L., Jr. *J. Am. Chem. Soc.* **1989**, *111*, 6183.
(50) Sugimoto, H.; Nagayama, T.; Maruyama, S.; Fujinami, S.; Yasuda, Y.; Suzuki, M.; Uehara, A. *Bull. Chem. Soc. Jpn.* **1998**, *71*, 2267.
(51) Suzuki, M. *Pure Appl. Chem.* **1998**, *70*, 955.
(52) Hayashi, Y.; Kayatani, T.; Sugimoto, H.; Suzuki, M.; Inomata, K.; Uehara, A.; Mizutani, Y.; Kitagawa, T.; Maeda, Y. *J. Am. Chem. Soc.* **1995**, *117*, 11220.
(53) Arii, H.; Nagatomo, S.; Kitagawa, T.; Miwa, T.; Jitsukawa, K.; Einaga, H.; Masuda, H. *J. Inorg. Biochem.* **2000**, *82*, 153.
(54) He, C.; Lippard, S. J. *Inorg. Chem.* **2001**, *40*, 1414.
(55) Kuzelka, J.; Spingler, B.; Lippard, S. J. *Inorg. Chim. Acta* **2002**, *337*, 212.
(56) (a) Mizoguchi, T. J.; Lippard, S. J. *J. Am. Chem. Soc.*, **1998**, *120*, 11022. (b) Mizoguchi, T. J.; Kuzelka, J.; Spingler, B.; DuBois, J. L.; Davydov, R. M.; Hedman, B.; Hodgson, K. O.; Lippard, S. J. *Inorg. Chem.* **2001**, *40*, 4662.
(57) Rebek, J., Jr.; Marshall, L.; Wolak, R.; Parris, K.; Killoran, M.; Askew, B.; Nemeth, D.; Islam, N. *J. Am. Chem. Soc.* **1985**, *107*, 7476.
(58) (a) Hagen, K. S.; Lachicotte, R.; Kitaygorodskiy, A. *J. Am. Chem. Soc.* **1993**, *115*, 12617. (b) Hagen, K. S.; Lachicotte, R.; Kitaygorodskiy, A.; Elbouadili, A. *Angew. Chem., Int. Ed. Engl.* **1993**, *32*, 1321.
(59) Herold, S.; Lippard, S. J. *J. Am. Chem. Soc.* **1997**, *119*, 145.
(60) Herold, S.; Lippard, S. J. *J. Am. Chem. Soc.* **1997**, *119*, 145.
(61) LeCloux, D. D.; Barrios, A. M.; Mizoguchi, T. J.; Lippard, S. J. *J. Am. Chem. Soc.* **1998**, *120*, 9001.
(62) Tolman, W. B.; Que, L., Jr. *J. Chem. Soc., Dalton Trans.* **2002**, 653.
(63) Lee, D.; Pierce, B.; Krebs, C.; Hendrich, M. P.; Huynh, B. H.; Lippard, S. J. *J. Am. Chem. Soc.* **2002**, *124*, 3993.
(64) Lee, D.; Lippard, S. J. *Inorg. Chem.* **2002**, *41*, 827.
(65) Lee, D.; Lippard, S. J. *Inorg. Chem.* **2002**, *41*, 2704.
(66) Lee, D.; Lippard, S. J. *J. Am. Chem. Soc.* **2001**, *123*, 4611.
(67) Lee, D.; Krebs, C.; Huynh, B. H.; Hendrich, M. P.; Lippard, S. J. *J. Am. Chem. Soc.* **2000**, *122*, 5000.
(68) Lee, D.; Du Bois, J.; Petasis, D.; Hendrich, M. P.; Krebs, C.; Huynh, B. H.; Lippard, S. J. *J. Am. Chem. Soc.* **1999**, *121*, 9893.
(69) Lee, D.; Lippard, S. J. *J. Am. Chem. Soc.* **1998**, *120*, 12153.
(70) Hagadorn, J. R.; Que, L., Jr.; Tolman, W. B. *Inorg. Chem.* **2000**, *39*, 6086.
(71) Hagadorn, J. R.; Que, L., Jr.; Tolman, W. B. *J. Am. Chem. Soc.* **1999**, *121*, 9760.
(72) Hagadorn, J. R.; Que, L., Jr.; Tolman, W. B. *J. Am. Chem. Soc.* **1998**, *120*, 13531.
(73) Chavez, F. A.; Ho, R. Y. N.; Pink, M.; Young, V. G., Jr.; Kryatov, S. V.; Rybak-Akimova, E. V.; Andres, H.; Münck, E.; Que, L., Jr.; Tolman, W. B. *Angew. Chem., Int. Ed.* **2002**, *41*, 149.
(74) (a) Barrios, A. M.; Lippard, S. J. *Inorg. Chem.* **2001**, *40*, 1060. (b) Barrios, A. M. Ph.D. Dissertation, Massachusetts Institute of Technology, Boston, 2000.
(75) Baik, M.-H.; Lippard, S. J.; Friesner, R. A. Unpublished results.
(76) (a) Kuzelka, J.; Farrell, J. R.; Lippard, S. J. *Inorg. Chem.* **2003**, *42*, 8652. (b) Farrell, J. R.; Stiles, D.; Lippard, S. J. Unpublished results.
(77) DeGrado, W. F.; Summa, C. M.; Pavone, V.; Nastri, F.; Lombardi, A. *Annu. Rev. Biochem.* **1999**, *68*, 779.
(78) Gibney, B. R.; Rabanal, F.; Dutton, P. L. *Curr. Opin. Chem. Biol.* **1997**, *1*, 537.
(79) Bryson, J. W.; Betz, S. F.; Lu, H. S.; Suich, D. J.; Zhou, H. X.; O'Neil, K. T.; DeGrado, W. F. *Science* **1995**, *270*, 935.
(80) DeGrado, W. F.; Wasserman, Z. R.; Lear, J. D. *Science* **1989**, *243*, 622.
(81) Baltzer, L.; Nilsson, J. *Curr. Opin. Biotechnol.* **2001**, *12*, 355.
(82) Summa, C. M.; Lombardi, A.; Lewis, M.; DeGrado, W. F. *Curr. Opin. Struct. Biol.* **1999**, *9*, 500.
(83) Maglio, O.; Nastri, F.; Pavone, V.; Lombardi, A.; DeGrado, W. F. *Proc. Natl. Acad. Sci. U.S.A.* **2003**, *100*, 3772.
(84) Hill, R. B.; Raleigh, D. P.; Lombardi, A.; DeGrado, W. F. *Acc. Chem. Res.* **2000**, *33*, 745.
(85) Lombardi, A.; Summa, C. M.; Geremia, S.; Randaccio, L.; Pavone, V.; DeGrado, W. F. *Proc. Natl. Acad. Sci. U.S.A.* **2000**, *97*, 6298.
(86) Pasternak, A.; Kaplan, J.; Lear, J. D.; DeGrado, W. F. *Protein Sci.* **2001**, *10*, 958.
(87) Di Costanzo, L.; Wade, H.; Geremia, S.; Randaccio, L.; Pavone, V.; DeGrado, W. F.; Lombardi, A. *J. Am. Chem. Soc.* **2001**, *123*, 12749.
(88) Marsh, E. N. G.; DeGrado, W. F. *Proc. Natl. Acad. Sci. U.S.A.* **2002**, *99*, 5150.
(89) Brown, C. A.; Remar, G. J.; Musselman, R. L.; Solomon, E. I. *Inorg. Chem.* **1995**, *34*, 688.
(90) Armstrong, W. H.; Spool, A.; Papaefthymiou, G. C.; Frankel, R. B.; Lippard, S. J. *J. Am. Chem. Soc.* **1984**, *106*, 3653.
(91) Armstrong, W. H.; Lippard, S. J. *J. Am. Chem. Soc.* **1983**, *105*, 4837.
(92) Wu, F.-J.; Kurtz, D. M., Jr.; Hagen, K. S.; Nyman, P. D.; Debrunner, P. G.; Vankai, V. A. *Inorg. Chem.* **1990**, *29*, 5174.
(93) Kodera, M.; Shimakoshi, H.; Nishimura, M.; Okawa, H.; Iijima, S.; Kano, K. *Inorg. Chem.* **1996**, *35*, 4967.
(94) Watton, S. P.; Masschelein, A.; Rebek, J., Jr.; Lippard, S. J. *J. Am. Chem. Soc.* **1994**, *116*, 5196.
(95) Trukhan, V. M.; Gritsenko, O. N.; Nordlander, E.; Shteinman, A. A. *J. Inorg. Biochem.* **2000**, *79*, 41.
(96) Ménage, S.; Galey, J.-B.; Dumats, J.; Hussler, G.; Seité, M.; Luneau, I. G.; Chottard, G.; Fontecave, M. *J. Am. Chem. Soc.* **1998**, *120*, 13370.

(97) Ménage, S.; Galey, J.-B.; Hussler, G.; Seité, M.; Fontecave, M. *Angew. Chem., Int. Ed. Engl.* **1996**, *35*, 2353.
(98) Westerheide, L.; Müller, F. K.; Than, R.; Krebs, B.; Dietrich, J.; Schindler, S. *Inorg. Chem.* **2001**, *40*, 1951.
(99) Scarpellini, M.; Neves, A.; Bortoluzzi, A. J.; Vencato, I.; Drago, V.; Ortiz, W. A.; Zucco, C. *J. Chem. Soc., Dalton Trans.* **2001**, 2616.
(100) Nie, H.; Aubin, S. M. J.; Mashuta, M. S.; Wu, C.-C.; Richardson, J. F.; Hendrickson, D. N.; Buchanan, R. M. *Inorg. Chem.* **1995**, *34*, 2382.
(101) Zheng, H.; Zang, Y.; Dong, Y.; Young, V. G., Jr.; Que, L., Jr. *J. Am. Chem. Soc.* **1999**, *121*, 2226.
(102) Zang, Y.; Dong, Y.; Que, L., Jr.; Kauffmann, K.; Münck, E. *J. Am. Chem. Soc.* **1995**, *117*, 1169.
(103) Zang, Y.; Pan, G.; Que, L., Jr.; Fox, B. G.; Münck, E. *J. Am. Chem. Soc.* **1994**, *116*, 3653.
(104) Marlin, D. S.; Olmstead, M. M.; Mascharak, P. K. *Inorg. Chem.* **2003**, *42*, 1681.
(105) Jensen, M. P.; Lange, S. J.; Mehn, M. P.; Que, E. L.; Que, L., Jr. *J. Am. Chem. Soc.* **2003**, *125*, 2113.
(106) Lange, S. J.; Miyake, H.; Que, L., Jr. *J. Am. Chem. Soc.* **1999**, *121*, 6330.
(107) Yoon, S.; Lippard, S. J. Unpublished results.
(108) Enomoto, M.; Aida, T. *J. Am. Chem. Soc.* **2002**, *124*, 6099.
(109) Fox, B. G.; Liu, Y.; Dege, J. E.; Lipscomb, J. D. *J. Biol. Chem.* **1991**, *266*, 540.
(110) DeWitt, J. G.; Bentsen, J. G.; Rosenzweig, A. C.; Hedman, B.; Green, J.; Pilkington, S.; Papaefthymiou, G. C.; Dalton, H.; Hodgson, K. O.; Lippard, S. J. *J. Am. Chem. Soc.* **1991**, *113*, 9219.
(111) Woodland, M. P.; Patil, D. S.; Cammack, R.; Dalton, H. *Biochim. Biophys. Acta* **1986**, *873*, 237.
(112) Dutta, S. K.; Ensling, J.; Werner, R.; Flörke, U.; Haase, W.; Gütlich, P.; Nag, K. *Angew. Chem., Int. Ed. Engl.* **1997**, *36*, 152.
(113) Cohen, J. D.; Payne, S.; Hagen, K. S.; Sanders-Loehr, J. *J. Am. Chem. Soc.* **1997**, *119*, 2960.
(114) Bossek, U.; Hummel, H.; Weyhermüller, T.; Bill, E.; Wieghardt, K. *Angew. Chem., Int. Ed. Engl.* **1995**, *34*, 2642.
(115) Que, L., Jr.; Dong, Y. *Acc. Chem. Res.* **1996**, *29*, 190.
(116) Dong, Y.; Ménage, S.; Brennan, B. A.; Elgren, T. E.; Jang, H. G.; Pearce, L. L.; Que, L., Jr. *J. Am. Chem. Soc.* **1993**, *115*, 1851.
(117) Ménage, S.; Brennan, B. A.; Juarez-Garcia, C.; Münck, E.; Que, L., Jr. *J. Am. Chem. Soc.* **1990**, *112*, 6423.
(118) Dong, Y.; Yan, S.; Young, V. G., Jr.; Que, L., Jr. *Angew. Chem., Int. Ed.* **1996**, *35*, 618.
(119) Feig, A. L.; Becker, M.; Schindler, S.; van Eldik, R.; Lippard, S. J. *Inorg. Chem.* **1996**, *35*, 2590.
(120) Feig, A. L.; Lippard, S. J. *J. Am. Chem. Soc.* **1994**, *116*, 8410.
(121) Suzuki, M.; Furutachi, H.; Okawa, H. *Coord. Chem. Rev.* **2000**, *200−202*, 105.
(122) Ookubo, T.; Sugimoto, H.; Nagayama, T.; Masuda, H.; Sato, T.; Tanaka, K.; Maeda, Y.; Okawa, H.; Hayashi, Y.; Uehara, A.; Suzuki, M. *J. Am. Chem. Soc.* **1996**, *118*, 701.
(123) Kitajima, N.; Tamura, N.; Amagi, H.; Fukui, H.; Moro-oka, Y.; Mizutani, Y.; Kitagawa, T.; Mathur, R.; Heerwegh, K.; Reed, C. A.; Randall, C. R.; Que, L., Jr.; Tatsumi, K. *J. Am. Chem. Soc.* **1994**, *116*, 9071.
(124) Kim, K.; Lippard, S. J. *J. Am. Chem. Soc.* **1996**, *118*, 4914.
(125) Brunold, T. C.; Tamura, N.; Kitajima, N.; Moro-oka, Y.; Solomon, E. I. *J. Am. Chem. Soc.* **1998**, *120*, 5674.
(126) Gherman, B. F.; Baik, M.-H.; Lippard, S. J.; Friesner, R. A. *J. Am. Chem. Soc.*, in press.
(127) Neese, F.; Solomon, E. I. *J. Am. Chem. Soc.* **1998**, *120*, 12829.
(128) Kryatov, S. V.; Rybak-Akimova, E. V.; MacMurdo, V. L.; Que, L., Jr. *Inorg. Chem.* **2001**, *40*, 2220.
(129) Kodera, M.; Taniike, Y.; Itoh, M.; Tanahashi, Y.; Shimakoshi, H.; Kano, K.; Hirota, S.; Iijima, S.; Ohba, M.; Okawa, H. *Inorg. Chem.* **2001**, *40*, 4821.
(130) Hummel, H.; Mekmouche, Y.; Duboc-Toia, C.; Ho, R. Y. N.; Que, L., Jr.; Schünemann, V.; Thomas, F.; Trautwein, A. X.; Lebrun, C.; Fontecave, M.; Ménage, S. *Angew. Chem., Int. Ed.* **2002**, *41*, 617.
(131) Duboc-Toia, C.; Ménage, S.; Ho, R. Y. N.; Que, L., Jr.; Lambeaux, C.; Fontecave, M. *Inorg. Chem.* **1999**, *38*, 1261.
(132) (a) Hazell, A.; Jensen, K. B.; McKenzie, C. J.; Toftlund, H. *Inorg. Chem.* **1994**, *33*, 3127. (b) Dong, Y.; Fujii, H.; Hendrich, M. P.; Leising, R. A.; Pan, G.; Randall, C. R.; Wilkinson, E. C.; Zang, Y.; Que, L., Jr.; Fox, B. G.; Kauffmann, K.; Münck, E. *J. Am. Chem. Soc.* **1995**, *117*, 2778.
(133) Dong, Y.; Que, L., Jr.; Kauffmann, K.; Münck, E. *J. Am. Chem. Soc.* **1995**, *117*, 11377.
(134) Hsu, H.-F.; Dong, Y.; Shu, L.; Young, V. G., Jr.; Que, L., Jr. *J. Am. Chem. Soc.* **1999**, *121*, 5230.
(135) Dong, Y.; Zang, Y.; Shu, L.; Wilkinson, E. C.; Que, L., Jr.; Kauffmann, K.; Münck, E. *J. Am. Chem. Soc.* **1997**, *119*, 12683.
(136) Kryatov, S. V.; Rybak-Akimova, E. V. *J. Chem. Soc., Dalton Trans.* **1999**, 3335.
(137) Zheng, H.; Yoo, S. J.; Münck, E.; Que, L., Jr. *J. Am. Chem. Soc.* **2000**, *122*, 3789.
(138) Siegbahn, P. E. M.; Crabtree, R. H. *J. Am. Chem. Soc.* **1997**, *119*, 3103.
(139) Shu, L.; Nesheim, J. C.; Kauffmann, K.; Münck, E.; Lipscomb, J. D.; Que, L., Jr. *Science* **1997**, *275*, 515.
(140) MacMurdo, V. L.; Zheng, H.; Que, L., Jr. *Inorg. Chem.* **2000**, *39*, 2254.
(141) Costas, M.; Rohde, J.-U.; Stubna, A.; Ho, R. Y. N.; Quaroni, L.; Münck, E.; Que, L., Jr. *J. Am. Chem. Soc.* **2001**, *123*, 12931.
(142) Grapperhaus, C. A.; Mienert, B.; Bill, E.; Weyhermüller, T.; Wieghardt, K. *Inorg. Chem.* **2000**, *39*, 5306.
(143) Mayer, K.; Bill, E.; Mienert, B.; Weyhermüller, T.; Wieghardt, K. *J. Am. Chem. Soc.* **1999**, *121*, 4859.
(144) Barton, D. H. R. *Tetrahedron* **1998**, *54*, 5805.
(145) Barton, D. H. R. *Chem. Soc. Rev.* **1996**, *25*, 237.
(146) Barton, D. H. R.; Doller, D. *Acc. Chem. Res.* **1992**, *25*, 504.
(147) Goldstein, S.; Meyerstein, D. *Acc. Chem. Res.* **1999**, *32*, 547.
(148) Walling, C. *Acc. Chem. Res.* **1998**, *31*, 155.
(149) MacFaul, P. A.; Wayner, D. D. M.; Ingold, K. U. *Acc. Chem. Res.* **1998**, *31*, 159.
(150) Sawyer, D. T.; Sobkowiak, A.; Matsushita, T. *Acc. Chem. Res.* **1996**, *29*, 409.
(151) Kim, C.; Dong, Y.; Que, L., Jr. *J. Am. Chem. Soc.* **1997**, *119*, 3635.
(152) Buist, P. H.; Behrouzian, B. *J. Am. Chem. Soc.* **1996**, *118*, 6295.
(153) (a) White, M. C.; Doyle, A. G.; Jacobsen, E. N. *J. Am. Chem. Soc.* **2001**, *123*, 7194. (b) Ryu, J. Y.; Kim, J.; Costas, M.; Chen, K.; Nam, W.; Que, L., Jr. *Chem. Commun.* **2002**, 1288.
(154) Mekmouche, Y.; Hummel, H.; Ho, R. Y. N.; Que, L., Jr.; Schünemann, V.; Thomas, F.; Trautwein, A. X.; Lebrun, C.; Gorgy, K.; Leprêtre, J.-C.; Collomb, M.-N.; Deronzier, A.; Fontecave, M.; Ménage, S. *Chem. Eur. J.* **2002**, *8*, 1196.
(155) (a) Yoon, S.; Lippard, S. J. *Inorg. Chem.* **2003**, *42*, 8606. (b) Carson, E. C.; Lippard, S. J., submitted for publication.
(156) Tshuva, E. Y.; Lee, D.; Bu, W.; Lippard, S. J. *J. Am. Chem. Soc.* **2002**, *124*, 2416.
(157) Moreira, R.; Tshuva, E. Y.; Lippard, S. J. Unpublished results.
(158) Guddat, L. W.; McAlpine, A. S.; Hume, D.; Hamilton, S.; de Jersey, J.; Martin, J. L. *Structure* **1999**, *7*, 757.
(159) Hempstead, P. D.; Hudson, A. J.; Artymiuk, P. J.; Andrews, S. C.; Banfield, M. J.; Guest, J. R.; Harrison, P. M. *FEBS Lett.* **1994**, *350*, 258.
(160) (a) deMaré, F.; Kurtz, D. M., Jr.; Nordlund, P. *Nat. Struct. Biol.* **1996**, *3*, 539. (b) Jin, S.; Kurtz, D. M., Jr.; Liu, Z.-J.; Rose, J.; Wang, B.-C. *J. Am. Chem. Soc.* **2002**, *124*, 9845.
(161) Lindqvist, Y.; Huang, W.; Schneider, G.; Shanklin, J. *EMBO J.* **1996**, *15*, 4081.
(162) Pikus, J. D.; Studts, J. M.; Achim, C.; Kauffmann, K. E.; Münck, E.; Steffan, R. J.; McClay, K.; Fox, B. G. *Biochemistry* **1996**, *35*, 9106.
(163) Cadieux, E.; Vrajmasu, V.; Achim, C.; Powlowski, J.; Münck, E. *Biochemistry* **2002**, *41*, 10680.
(164) Small, F. J.; Ensign, S. A. *J. Biol. Chem.* **1997**, *272*, 24913.
(165) Sluis, M. K.; Sayavedra-Soto, L. A.; Arp, D. J. *Microbiology* **2002**, *148*, 3617.
(166) Hsu, H.-F.; Que, L., Jr.; Shanklin, J. *J. Inorg. Biochem.* **1999**, *74*, 168.
(167) Rea, S. *FEBS Lett.* **2001**, *509*, 389.
(168) Foster, T. L.; Caradonna, J. P. *J. Am. Chem. Soc.*, **2003**, *125*, 3678.

CR020622Y